ELSEVIER

Contents lists available at ScienceDirect

European Journal of Pharmacology

journal homepage: www.elsevier.com/locate/ejphar





Kinetics of thymic regeneration in female mice following short-term rapamycin administration

Fengjie Zhang, Shiyu Hu, Yuyuan Ying, Meiru Zhou, Xunuo Wen, Qingru Sun, Zhaohuan Lou *6, Jianli Gao **6

School of Pharmaceutical Sciences, Zhejiang Chinese Medical University, Hangzhou, 310053, Zhejiang, PR China

ARTICLE INFO

Keywords: Thymic involution Thymic regeneration Rapamycin IL-7 Metformin

ABSTRACT

Thymus is the core organ that reflects the degree of aging, and the anti-aging effect of rapamycin(RAPA) has been confirmed by multiple studies, but the dynamic changes of the thymus after the administration of RAPA have been lacking systematic research. Here, we observed the involution of thymus induced by RAPA (1 mg/kg/day, i. p. for 3 days) and its regeneration kinetics after withdrawal of RAPA, to explore the possible mechanism of RAPA's anti-aging effects based on changes in thymus function. The results show that the thymus weight decreased by 46.15% post-RAPA, then regenerated from 20.45 mg to 57.97 mg, reaching 1.3-fold baseline levels in age-matched controls. RAPA can cause acute involution in thymic structure and function, such as loss of medullary thymic epithelial cells (mTECs) and subcapsular thymic epithelial cells (sTECs), abnormal differentiation of thymocytes, reduction of peripheral T cell proportion, and up-regulation of Foxn1 and Klf6 mRNA levels. Regeneration featured expanded double positive (DP) T cells, CD3⁺TCRβ⁺ T cells, CD8 single-positive (SP) T cells, medullary dilatation, and thymocyte telomere elongation. IL-7 and MET have pro-regeneration effects, but neither of them could accelerate RAPA-mediated thymic regeneration. IL-7 can prolong telomere length of thymocytes and restore peripheral T cell homeostasis, while MET can promote T cell positive selection and increase Sirt3 and Gimap4 mRNA levels. These results demonstrate that RAPA triggers transient thymic suppression followed by thymus volume and functional recovery. It seems that RAPA-mediated immune reconstitution may be an important reason for the potential anti-aging effect of RAPA.

1. Introduction

Rapamycin(RAPA) is a macrolide antibiotic and is widely used in clinical practice(Choudhury et al., 2024; Kraaijeveld et al., 2019). Emerging evidence suggests that RAPA modulates cellular proliferation and differentiation via the mTOR signaling pathway, thereby extending lifespan and mitigating age-related pathologies(Chen et al., 2009; Weichhart, 2018). In elderly populations, short-term RAPA administration enhances immune competence, remodels the microbiota, and exerts sustained anti-aging effects persisting for at least three months post-treatment(Bitto et al., 2016). Intriguingly, even in young individuals, transient RAPA exposure has demonstrated anti-senescence benefits(Breed et al., 2018). Despite these findings, the dynamic alterations in thymic architecture and concomitant T-cell immunity after short-term application of RAPA in adolescence are still lacking in exploration.

Thymus, the first organ to show age-related changes in human body, regresses with age after puberty reaches its peak(Boehm et al., 2013). The thymic output of memory T cells in aging thymus decreases, the diversity of TCR library shrinks, and immune dysfunction and immunosenescence occur(Thomas et al., 2020). As an important central immune organ, it is mainly composed of thymic stromal cells and thymocytes. Thymic epithelial cells (TEC) is the most important type of thymic stromal cell. And the thymus function is mainly coordinated by TEC, which is usually divided into capsule, subcapsule area, cortical area, cortex-medullary junction area and medullary area according to tissue characteristics(Nitta et al., 2020). This structural compartmentalization underpins the thymic microenvironment essential for T-cell development and selection.

Thymic involution can be triggered by oxidative stress, infection, or radiation, yet regenerative processes often ensue upon cessation of these stressors(Ashby et al., 2023; Cosway et al., 2023; Miller, 2020). Notably,

^{*} Corresponding author. No.548 Bin Wen Road, Binjiang Dist., Hangzhou, Zhejiang Province, 310053, PR China.

^{**} Corresponding author. No.548 Bin Wen Road, Binjiang Dist., Hangzhou, Zhejiang Province, 310053, PR China. *E-mail addresses*: zhaohuanlou@zcmu.edu.cn (Z. Lou), jianligao@zcmu.edu.cn (J. Gao).

thymic regeneration therapies have shown promise in attenuating aging phenotypes and age-associated diseases. Intriguingly, the anti-aging efficacy of RAPA may partially arise from thymic rejuvenation following transient treatment(Fahy et al., 2019; Abbott, 2024). To systematically delineate the temporal dynamics of RAPA-induced thymic remodeling, we employed a short-term low-dose RAPA regimen (1 mg/kg/d, i.p. for 3 days) in 6-8 weeks female mice. This way allowed characterization of acute thymic involution and subsequent natural regeneration kinetics at 3 and 14 days post-withdrawal. In fact, endogenous thymic regeneration is regulated by TEC, thymocyte proliferation and apoptosis(Duah et al., 2021; Liang et al., 2022). Interleukin-7 (IL-7) and metformin (MET), pivotal regulators of thymic homeostasis, exhibit therapeutic potential in preserving thymic function and counteracting immunosenescence. IL-7 deficiency leads to profound thymic hypoplasia, while exogenous IL-7 supplementation partially reverses age-related thymic involution(Barata et al., 2019; Chaudhry et al., 2016). Similarly, Xu's research shows that MET could increase thymus volume, and another study shows that MET ameliorates D-galactose-induced thymic involution via mitochondrial function modulation(Liu et al., 2023; Xu et al., 2024). Building on these insights, we further investigated whether IL-7 or MET administration could augment endogenous thymic regeneration post-RAPA withdrawal, aiming to elucidate their mechanistic roles in this process.

In summary, this study provides a comprehensive analysis of thymic dynamics following short-term, low-dose RAPA exposure, integrating multimodal assessments of regenerative kinetics and therapeutic interventions(e.g. IL-7/MET). Our findings advance the understanding of thymus-centric mechanisms underlying RAPA-mediated anti-aging effects, offering a foundation for thymic regeneration therapies to promote immune reconstitution.

2. Materials and methods

2.1. Animals and experimental design

Female BALB/c mice (6–8 weeks old) were purchased from Shanghai Slack Co., Ltd. (license number, SCXK(Hu)2022-0004) and all mice were housed in a controlled environment (room temperature 26 \pm 2 $^{\circ}$ C, humidity 30 \pm 5%, light-dark cycle 12/12 h) at the Animal Center of Zhejiang Chinese Medical University. One day prior to the start of the experiment, the animals were depilated on the dorsal region using depilatory cream.

All experiments were approved by the Professional Committee for Animal Ethics and Welfare of Zhejiang Chinese Medical University (Ethics Approval No. IACUC-20230814-04) and conducted in accordance with the guidelines for laboratory animal care (AAALAC accreditation).

RAPA was used experimentally (1 mg/kg/day, intraperitoneal, A2221042, Shanghai Aladdin Biochemistry Co., Ltd., China; purity \geq 98%), Metformin hydrochloride (MET) (100/300 mg/kg, intraperitoneal injection, BSC188, Beijing Bide Pharmaceutical Technology Co., Ltd., China; purity, 97%), Recombinant Mouse IL-7 (0.5 µg/mouse, intraperitoneal injection every other day, P5930, Beyotime, China, purity >96%).

The composition and correspondence of our animal experiment establishment are briefly described as follows, Nor (Normal), Rap (RAPA), RR1 (RAPA+0.9% NaCl-3 days), RR2 (RAPA+0.9% NaCl-14 days), RI1 (RAPA + IL-7-3 days), I1 (0.9%NaCl + IL-7-3 days), RI2 (RAPA + IL-7-14 days), I2 (0.9% NaCl + IL-7-14 days), RML1 (RAPA + MET-L-3 days), RML2 (RAPA + MET-L-14 days), RMH1 (RAPA + MET-H-3 days), RMH2 (RAPA + MET-H-14 days), ML1 (0.9% NaCl + MET-L-3 days), ML2 (0.9% NaCl + MET-L-14 days).

2.2. Experimental cells

Immortalized BALB/c mouse thymic epithelial cells were

constructed by our group(Shen et al., 2020). iTEC (Immortalized thymic epithelial cells) cells were cultured using high glucose medium (C11995500BT, Gibco, Tokyo, Japan) containing 5% fetal bovine serum (11011-8611, EVERY GREEN Nagano, Japan) and 1% dual antibody (CR-15140, Cienry, Huizhou, China) and incubated in a constant temperature carbon dioxide incubator (Forma 310, Thermo Fisher Scientific, Waltham, MA, USA) at 37 $^{\circ}\mathrm{C}$ in an environment of 5% carbon dioxide.

Thymocytes were obtained from fresh thymus of BALB/c mice (6–8 weeks old, female). Fresh thymus was washed with PBS containing 1% bispecific antibody, and then the thymus was cut open with sterile scissors. Thymocytes were squeezed out gently with sterile pestle, and centrifuged at 1500 rpm for 2 min to collect thymocytes. The culture conditions were the same with iTEC.

2.3. Body weight and thymus index

In this experiment, the weight of mice was recorded every day, and mice ate and drank freely. The thymus at the upper part of the anterior mediastinum behind the sternum was obtained at different time periods. The connective tissue around the thymus was carefully removed and the wet weight of the thymus was weighed using an electronic balance. Thymus index (%) = thymic wet weight (g)/mouse weight (g) \times 100%, and then statistics were performed.

2.4. Whole blood biochemical indexes measurement

At the end of the experiment, mice were anesthetized with isophorane and blood samples were taken from their orbits. A total 150 μL of peripheral blood was taken into EDTA containing anticoagulant tubes and mixed well. The ratio of lymphocytes and neutrophils in routine blood was examined by using an automatic blood analyzer (SYSMEX, Japan).

2.5. Histological examination(H&E)

Thymic tissue was fixed in 10% formalin solution for 48 h, dehydrated in a total enclosure tissue dehydrator, embedded in paraffin, and then cut into 4 μm sections by LEI-CARM2245 microtome (Leica Microsystems Nussloch GmbH, Germany). Thymic tissue sections were routinely dewaxed and hydrated, hematoxylin-eosin stained, and pictures were obtained using a common microscope for histopathological analysis.

2.6. Immunofluorescence(IF)

Paraffin sections of thymus were routinely dewaxed and hydrated, slides placed in EDTA antigen retrieval solution (50X)(ZLI-9069, ZSGB-Bio, China) and deionized water (1:50 dilution) were heated in a microwave oven for repair, followed by addition of rabbit anti-mouse cytokeratin 8 (CK8, GR31819624, Abcam, UK, 1:150 dilution) and mouse monoclonal cytokeratin 5 (CK5, 57u2005, Affinity Biosciences, China; 1150 dilution) were incubated for 16 h at 4 °C. CD4 (Abcam, ab28872, 1:50 dilution) and CD8 (STARTER, S0B0034, 1:150 dilution) were used to detect in situ fluorescence. Bcl-2 (Santa Cruz, 0492, 1:150 dilution) and Bax (Abmart, T40051M, 1200 dilution) antibodies were used to detect apoptosis cells in thymus. Through the IF staining of Bcl-2 (cyan) and Bax (orange) in thymus tissue, the frame selection of the touched area and the non-touched area of the thymus was carried out. And then the results were obtained according to the formula, the degree of apoptosis = FTTC channel fluorescence value/AF555 fluorescence channel value. These antiboties were detected with Co-staining of A and B was performed using a Four color mIHC Fluorescence kit (Recordbio Biological Technology, Shanghai, China) based on the tyramide signal amplification (TSA) technology according to the manufacture's instruction. Images were captured using Zeiss upright fluorescence

microscope (AXIO SCOPE. A1).

2.7. Flow cytometry

2.7.1. T cell subsets in thymus

Fresh thymus was ground gently and thymocyte suspension was sieved through a 70 μm cell sieve. Thymocytes were then centrifuged at 2000 rpm for 6 min, supernatant discarded and resuspended in 200 μL PBS solution, then incubated with CD3 FITC(553061), CD4 APC (553051), CD8 PE(553032) and TCR β Percp5.5 (H57-597) antibodies (all from BD Pharmingen, San Diego, CA, USA) for 40 min in the dark at 4 °C, washed once with PBS, then resuspended in 400 μL PBS solution and detected using flow cytometry (CytoFLEX Beckman, USA).

2.7.2. The proportion of CD3 $^+$ T cells and CD34 $^+$ cells in peripheral blood After the mice were anesthetized with isoflurane, orbital blood was taken into anticoagulant tubes containing heparin (EDTA), centrifuged at $1000 \times g$ for 5 min, the supernatant serum was discarded, and then lysed with erythrocyte lysate at room temperature. After centrifugation at $450 \times g$, the supernatant was discarded and resuspended in $300 \, \mu L$ PBS. A portion was added with CD3 APC (553066) and CD34 FITC (553733) antibodies (all from BD Pharmingen, San Diego, CA, USA) and incubated for 30 min at 4 $^\circ$ C in the dark. PBS was washed once, and then the cells were resuspended in 300 μL PBS solution for detection by flow cytometry (CytoFLEX Beckman, USA).

2.8. TRECs level in peripheral blood

The lysed blood cell suspension was washed once with PBS, peripheral blood DNA was extracted using Mammalian DNA Extraction Kit (D0061, Beyotime, Shanghai, China), and then T cell receptor excision loops (*TRECs*) in peripheral blood mononuclear cells were quantified by qRT-PCR to evaluate thymic export function.

2.9. Determination of telomere length in Thymocyte

DNA was extracted from thymocytes according to the manual of Mammalian DNA Extraction Kit (D0061, Beyotime, Shanghai, China), and standard samples were prepared by taking multiple samples of the same amount. Two standard curves of 36B4F and Tel were drawn according to Log value of DNA content in each well and Ct value of corresponding 36B4F/Tel gene under different concentrations of standard samples($R^2 > 0.95$). The linear regression equation of 36B4F and Tel is obtained; according to the sample containing 10 ng DNA in each well, the fixed values Ct_0 (Tel) and Ct_0 (Tel) are calculated according to the two standard curves, and finally the Ct values of Tel genes of different samples are brought into the calculation formula of relative telomere length for calculation, so that the relative telomere length of different samples can be obtained, Relative Telomere Length = Relative $Tel/S = 2^{-[CCt(T)-Ct0 (T))-(Ct(S)-Ct0 (S))]}$.

2.10. Real-time RT-PCR

2.10.1. Thymus tissue

Detection of mRNA levels in thymus by qRT-PCR. The mRNA levels of thymosin $\beta 4(T\beta 4)$, thymosin $\beta 15(T\beta 15)$, thymosin $\alpha 1(T\alpha 1)$ and thymic stromal lymphopoietin(Tslp) and senescence-associated secretory phenotype (SASP) factors Interleukin- $1\alpha(IL-1\alpha)$, Interleukin- $1\beta(IL-1\beta)$, Interleukin-6(IL-6), and Cellular Tumor Antigen P53 (P53), Cyclin dependent kinase inhibitor 1A(P21), Sirtuin3(Sirt3), Sirtuin6(Sirt6), C-X-C motif chemokine ligand 12(CXCL12) mRNA levels in thymus. The mRNA levels of intercellular cell adhesion molecule-1 (ICAM-1), $vascular\ cell\ adhesion\ molecule\ 1(VCAM-1)$ and positive selection related genes IMAP Family Member 3(Gimap3), $IMAP\ Family\ Member\ 4(Gimap4)$, histocompatibility 2, K1, K region(H2-K1), beta-2 microglobulin($\beta 2m$) were also detected.

2.10.2. iTECs

Different groups, namely Nor (Normal), Rap (RAPA), RR (RAPA + normal medium), RI (RAPA + IL-7), RML (RAPA + MET-L), RMH (RAPA + MET-H), ML (MET-L) groups were set up. iTEC was treated with RAPA (20 nM) for 24 h, and then the RR group was replaced with normal medium, RI was replaced with medium containing IL-7 (0.5 μ g/mL), RML and RMH groups were replaced with medium containing MET (0.1 μ M), respectively, ML group was replaced with medium containing MET (0.1 μ M). After 24 h of culture, RNA was extracted and Krüppel-Like Factor 6 (*Klf6*), Forkhead Box Protein N1 (*Foxn1*), Autoimmune Regulator (*Aire*) mRNA levels were detected.

2.10.3. Thymocytes

Thymocytes were cultured in DMEM medium containing 5% Fetal bovine serum and 1% Penicillin-Streptomycin Solution for 4 h in carbon dioxide incubator. Thymocytes RNA was extracted and T-helperinducing POZ-p1(Thpok-p1), T-helper-inducing POZ-p2(Thpok-p2), GATA-binding protein 3(GATA3), Runt-related transcription factor 3 (Runx3) mRNA levels were detected. Groups were set up as Nor, Rap(10 nM), Rap(20 nM), IL-7 (0.5 μ g), IL-7 (0.05 μ g), MET (0.1 μ M), MET (1 μ M).

Frozen thymus(Store in refrigerator at minus 80 °C) was taken and total RNA was extracted using Tissue RNA Rapid Extraction Kit (Tissue, RN001, Shanghai Yishan Biotechnology Co., Ltd., China) according to manufacturer's instructions. cDNA was obtained by reverse transcription using Rapid Reverse Transcription Kit(Tissue, RT001, Shanghai Yishan Biotechnology Co., Ltd., China). mRNA levels in thymus was detected using SYBR Green qPCR premix, ABI PRISM 7500 Real-Time PCR System (Applied Biosystems) instrument, *GAPDH* as internal reference, and relative quantification using $2^{-\Delta\Delta Ct}$ data processing method according to manufacturer's instructions. Gene primers were synthesized and prepared by Sangon Bioengineering (Shanghai) Co., Ltd (Shanghai, China) (see Table 1 for sequences).

2.11. Transmission electron Microscope(TEM)

The ultrastructure of thymus was observed by transmission electron microscope. Thymus (1 \times 1 \times 1 mm) was fixed in 2.5% glutaraldehyde in 0.1 M sodium cacodylate buffer, pH 7.4, and dehydrated with a series of graded concentrations of ethanol and acetone. Tissues were embedded in epoxy-filled capsules, cut into ultrathin sections (60–80 nm) by an ultrathin microtome, and stained with uranyl acetate and lead citrate. Ultrastructural images of the thymus were captured using TEM (H7650, Hitachi, Japan).

2.12. Statistical analysis

Graphpad Prism 8.0.1 statistical software was used for analysis. T test was used for comparison between the two groups, and one-way ANOVA was used for comparison among multiple samples. The experimental results were expressed in the form of $\overline{x} \pm s$, P > 0.05 was not significant and had no statistical significance. Compared with "Nor" group, **P < 0.01, *P < 0.05. Compared with "Rap" group, **P < 0.01, *P < 0.05. Compared with "RR1" group, *P < 0.01, *P < 0.05. Compared with "RR2" group, *P < 0.05. Compared with "RR2" group, *P < 0.05.

3. Results

3.1. Acute regression of thymus induced by short-term RAPA

In recent years, RAPA has been widely concerned because of its potential positive effect on aging. It is highly likely related to the influence of its different treatment forms on thymic structure and function focuses on thymocyte differentiation, apoptosis and thymic epithelial cell distribution(Juricic et al., 2022; Wilkinson et al., 2012; Zhuo et al., 2022). RAPA prolonged lifespan in both aging and young mice, and it

Table 1List of primer sequences.

Gene Names	Primer sequences (5'-3')	Gene Names	Primer sequences (5′–3′)
GAPDH	F,5'-GGCTGCCCAGAACATCAT-3'	Aire	F,5'-AGGTCAGCTTCAGAGAAAAC-3'
	R,5'-CGGACACATTGGGGGTAG-3'		R,5'-TCATTCCCAGCACTCAGTAGA-3'
Τβ4	F,5'-TGACAAACCCGATATGGCTGA-3'	Foxn1	F,5'-TCACCTGATGTCAGCCCAGA-3'
	R,5'-ATTCGCCAGCTTGCTTCTCT-3'		R,5'-CGAAGAAAGCCAGCTGCTCA-3'
Τβ15	F,5'-TTGGAACCGGCAGACAAGATG-3'	Klf6	F,5'-ACTGTCTTTTCCAACCCGAC-3'
	R,5'-ATCTACCAGGAGCTGCCTAACA-3'		R,5'-AAGATAGCGTTCCAACTCCAG-3'
Τα1	F,5'-TAACCTTACGCACCGTGACC-3'	Gimap3	F,5'-TCATGCCGAGACACTCCTTAG-3'
	R,5'-GGTGGAGAGCGCATGTCATA-3'	-	R,5'-CAACACCTCCAACTTTTTGCC-3'
Tslp	F,5'-AGCCAGCTTGTCTCCTGAAA-3'	Gimap4	F,5'-CGGGGTTCATCCCAGAAAGTT-3'
	R,5'-GGCAAATGTTTTGTCGGGGA-3'	-	R,5'-CCCCAAGGATACTGTTCCCTG-3'
Sirt3	F,5'-TGCCTGCAAGGTTCCTACTC-3'	H2-K1	F,5'-ACCAGCAGTACGCCTACGA-3'
	R,5'-AGTCGGGGCACTGATTTCTG-3'		R,5'-AACCAGAACAGCAACGGTCG-3'
Sirt6	F,5'-AAGTCTCACTGTGTCCCTTGTC-3'	β 2 m	F,5'-TTCTGGTGCTTGTCTCACTGA-3'
	R,5'-TCACGAGCGGGTGTGATTG-3'		R,5'-CAGTATGTTCGGCTTCCCATTC-3'
P53	F,5'-GTACCTTATGAGCCACCCGA-3'	VCAM-1	F,5'-CTCTTACCTGTGCGCTGTGA-3'
	R,5'-ATGGTAAGGATAGGTCGGCG-3'		R,5'-GACAGGTCTCCCATGCACAA-3'
P21	F,5'-CCTGGTGATGTCCGACCTG-3'	ICAM-1	F,5'-GTGATGCTCAGGTATCCATCCA-3'
	R,5'-CCATGAGCGCATCGCAATC-3'		R,5'-CACAGTTCTCAAAGCACAGCG-3'
<i>IL</i> -1α	F,5'-AAGTCTCCAGGGCAGAGAGG-3'	Thpok-p1	F,5'-CAGGTGAATGTACGGCTCTC-3'
	R,5'-TTTCTTTGCCGACTCAAGCG-3'		R,5'-ATCTTCTCCTTTCAGCCGTTG-3'
IL-1 β	F,5'-CACCAGCACATTGCTTTGATGA-3'	Thpok-p2	F,5'- TTGCCGGCAAGGCCCCTCAGCGTTC-3'
	R,5'-GGAGCCTCATGGCCCAATTT-3'		R,5'- GAAGTAGTGGCTACAGGCAGCC-3'
IL-6	F,5'-TGAACTCCTTCTCCACAAGCG-3'	GATA3	F,5'-TTATCAAGCCCAAGCGAAG-3'
	R,5'-GCCTCTTTGCTGCTTTCACA-3'		R,5'-CATTAGCGTTCCTCCAG-3'
Runx3	F,5'-ACAGCATCTTTGACTCCTTCC-3'	CXCL12	F,5'-TGCATCAGTGACGGTAAACCA-3'
	R,5'-TGTTCTCGCCCATCTTGC-3'		R,5'-CACAGTTTGGAGTGTTGAGGAT-3'
36B4F	F,5'-ACTGGTCTAGGACCCGAGAAG-3'	Tel	F,5'-CGGTTTGTTTGGGTTTGGGTTTGGGTTTGGGTT-3'
	R,5'-TCAATGGTGCCTCTGGAGATT-3'		R,5'-GGCTTGCCTTACCCTTACCCTTACCCTTACCCT-3'

showed different benefits in a variety of models.

3.1.1. Short-term RAPA administration reduces thymic medulla area, decreases mTECs and sTECs number

RAPA has a significant inhibition on thymus. By intraperitoneal injection of RAPA for 3 days (Fig. 1A), we found that 1 mg/kg RAPA reduced thymus index by about 50.3%, from 44.3 mg to 20.5 mg (thymus wet weight, P < 0.01) and 0.201%–0.100% (thymus index, P < 0.01) (Fig. 1B). Histological analysis revealed disrupted cortex-medullary demarcation and medullary degeneration in RAPA-treated thymic, contrasting sharply with the well-defined cortex-medullary architecture observed in Nor group (Fig. 1C). Flow cytometric analysis further demonstrated significant thymocyte depletion with reduced cell discard rates compared to Nor group (Supplementary Fig. 2A and 2B).

TEC is mainly divided into cortical thymic epithelial cells (cTEC) and medullary thymic epithelial cells (mTEC). Keratin 5/8 (CK5/8) is the surface marker of mTEC and cTEC respectively. Multiple fluorescent staining (TSA) revealed reduced CK5 expression and decreased CK8 expression in the cortex in Rap group compared with Nor group (Fig. 1D). Previous studies have also shown that loss of mTOR leads to a decrease in mTEC(Liang et al., 2021). Further observation in the second image of Fig. 1D showed that the distribution of reticular mTEC decreased. As shown in the third image of Fig. 1D, RAPA enhances the thickness of the thymus envelope and reduces the number of TEC in the subcapsular region. Given that early T cell progenitor cells (ETPs) differentiate into DN T cells (CD4-CD8-, Double-Negative) under the subcapsular membrane and further differentiate and mature under the guidance of TEC(Wang et al., 2011). The application of RAPA results in the deletion of subcapsular TEC (sTEC) and provides a explanation for impaired T-cell development of DN to DP(CD4⁺CD8⁺, Double-Positive).

3.1.2. Short-term RAPA administration decreases thymic function

Recent studies have highlighted the pivotal role of thymic stromal cells in age-related thymic involution. Krüppel-like factor 6 (*Klf6*), a critical regulator of TEC development, promotes the distribution of specific TEC subsets essential for thymic function(Malin et al., 2023). The data demonstrate that RAPA administration significantly

upregulates mRNA levels of *Aire* (which governs tissue-restricted antigen(TRA) expression)(P < 0.01)(Fig. 1F)(Wang et al., 2011). Thymic stromal cells make an important contribution to the thymic microenvironment, and tight junctions between thymocytes are an evaluation of normal thymic structure(Nagatake et al., 2021). Transmission electron microscopy(TEM) analysis revealed ultrastructural alterations in RAPA-treated thymus, including reduced desmosomal junctions between thymocytes and increased senescent mitochondria. Paradoxically, results only shouwed significantly elevated mRNA levels of adhesion molecules VCAM-1 (Fig. 1E and G). RAPA specifically regulated $T\beta15$ and $T\alpha1$ mRNA levels, $T\beta15$ was significantly decreased and $T\alpha1$ was significantly increased(Fig. 1H). These findings collectively indicate that RAPA exerts its effects on thymic function primarily through modulation of thymic epithelial cells, establishing a complex interplay between structural remodeling and molecular regulation.

3.1.3. Short-term RAPA decreases DP T cells ratio, and promotes positive selection of DP to SP $\,$

Flow cytometry and multiple fluorescent staining results indicated that Rap group significantly increased the ratio of CD3⁺, CD3⁺TCRβ⁺, CD8SP (CD3⁺TCRβ⁺CD4⁻CD8⁺, CD8 Single-Positive) and ISP8 (CD3⁻TCRβ⁻CD4⁻CD8⁺, Immature CD8 Single-Positive) T cells (P < 0.01), but decreased the ratio of DP T cells by about 41% (P < 0.01) (Fig. 2A and B). Cortical and medullary parts of the thymus play different roles in thymocyte development, with TECs acting as central participants in positive selection processes(Wang et al., 2011). The mRNA levels of Gimap3, Gimap4, H2-K1, and β 2m related to positive selection in thymus were significantly increased(Fig. 2C). Thpok-p1, Thpok-p2, GATA3, Runx3 are critical in the subsequent negative selection process of DP T cells. And RAPA promotes the mRNA levels of *Thpok* and GATA3 genes in thymocytes, but high levels of CD4SP T cells are not observed in flow cytometry(Fig. 2D). Instead, RAPA selects towards CD8SP T cells, which is closely related to Runx3 activation of CD8 locus and silencing of CD4 locus.

Immunofluorescence(IF) localization of CD4 and CD8 revealed that Rap group exhibited a concentration of CD8 positive cells within the subcapsular cortex(Fig. 2E). Concurrently, although anti-apoptotic

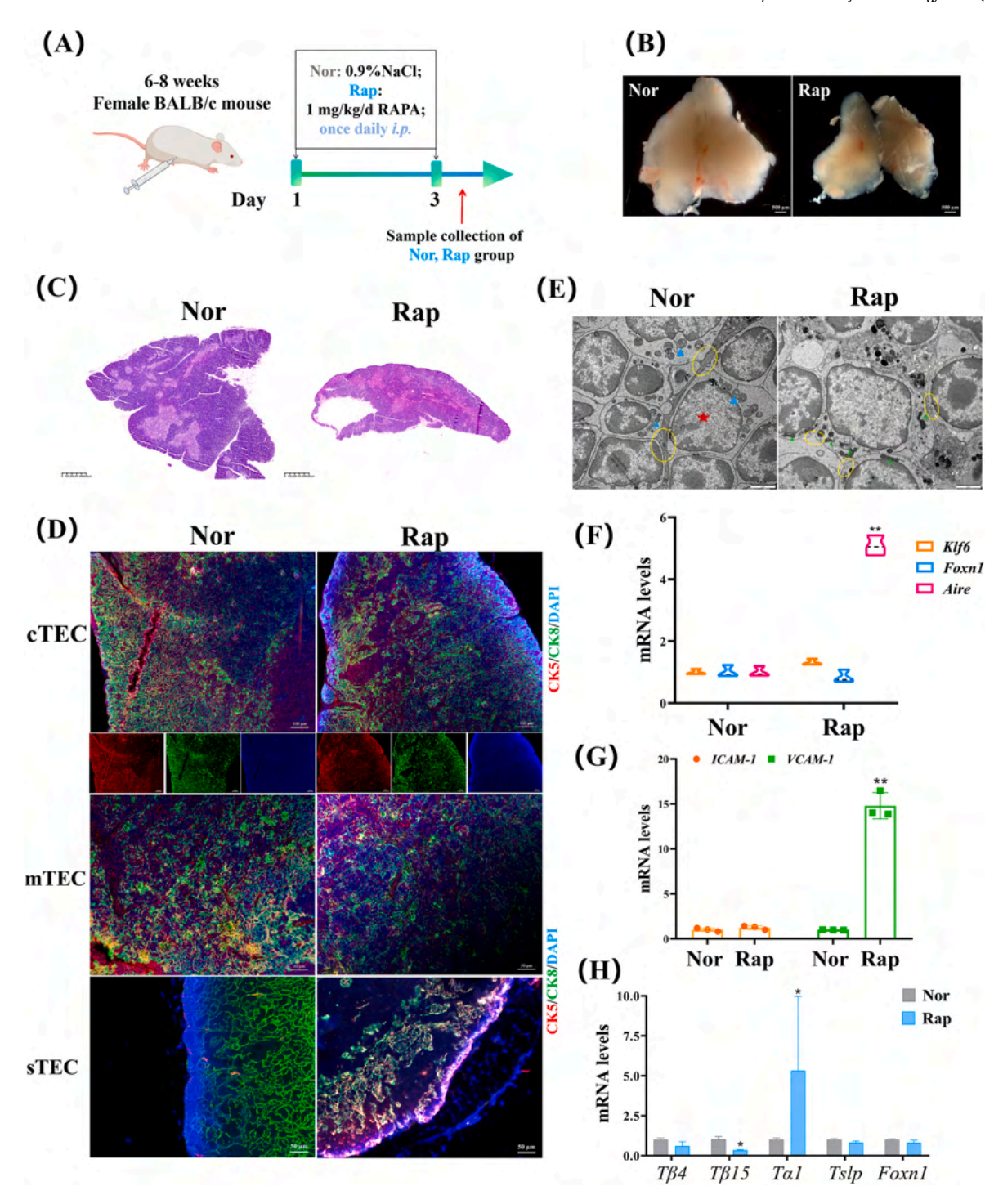


Fig. 1. Effects of short-term RAPA on structure and function of thymus. (A) Experimental design diagram of RAPA-induced acute degeneration of thymus. (B) Representative diagram of thymus organs of RAPA-induced acute degeneration of thymus. (C) H&E staining picture of thymus, scale bar = 625 μ m(25 \times), darker staining area is thymus cortex, lighter staining area is thymus medulla. (D) Spatial distribution changes of TECs of thymus induced by RAPA (CK5, red; CK8, green). cTEC, scale bar = 100 μ m. mTECs, scale bar = 50 μ m, the white dotted line framed part is reticular TECs. sTECs, Scale bar = 20 μ m. (E) Transmission electron microscope was used to observe the ultrastructural changes of thymus. Blue arrows represent the normal morphology of mitochondria in thymocytes, green arrows represent the senescent morphology of mitochondria in thymocytes, and yellow circles represent the tight junctions between adjacent thymocytes. (F) mRNA levels of *Klf6, Foxn1, Aire* genes related to iTEC function, n = 6. (G) mRNA levels of *ICAM-1* and *VCAM-1* in thymus, n = 6. (H) mRNA levels of $T\beta4$, $T\beta15$, $T\alpha1$, Tslp and Ta1 in thymus, Ta1 in

protein expression changed with no significant in the subcapsular region and the non-subcapsular regions(Fig. 2F and G). Consistent with prior findings(Takaba et al., 2017), which demonstrate that the interaction between TCR of DP T cells and antigen peptide-MHC I molecular complex on TEC drives CD8 positive T cells lineage commitment. Based of

the change in anti-apoptotic within non-subcapsular TECs, coupled with an increase in thymic output (as measured by *TRECs*, Fig. 2H), provides a potential mechanistic explanation for the significantly higher proportion of CD8SP T cells.

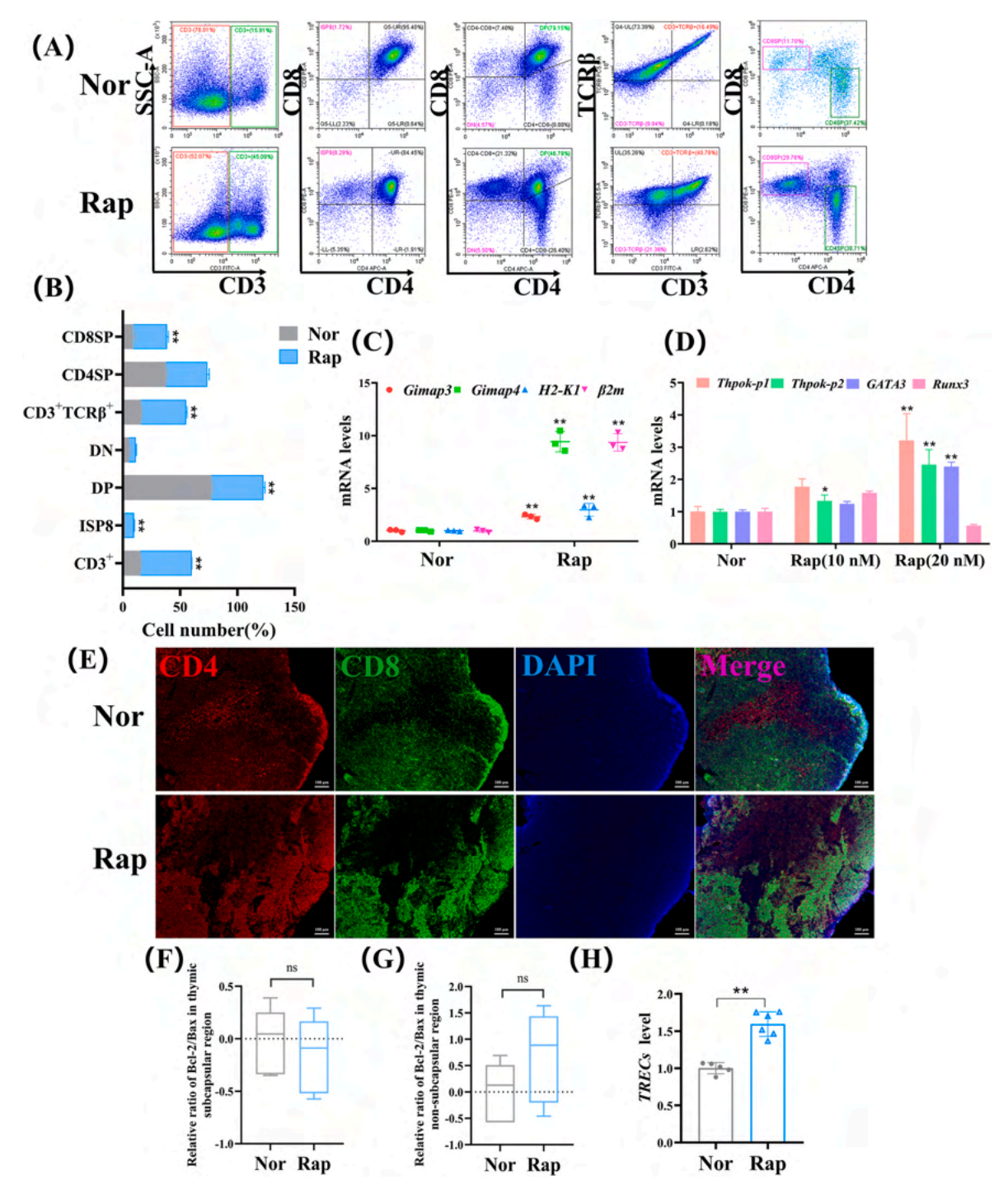


Fig. 2. Short-term RAPA affects T cell subsets distribution. (A) Flow cytometry of thymocyte CD3⁺, CD3⁺TCR β ⁺, DP (CD4⁺CD8⁺), DN (CD4⁻CD8⁻), CD4SP (CD3⁺TCR β ⁺CD4⁻CD8⁻), CD8SP (CD3⁺TCR β ⁺CD4⁻CD8⁺), ISP8 (CD3⁻TCR β ⁻CD4⁻CD8⁺). (B) T cell subsets were counted by flow cytometry, n=3. (C) mRNA levels of positive selection related genes *Gimap3*, *Gimap4*, *H2-K1*, β 2m in thymus, n=3. (D) mRNA levels of negative selection related genes *Thpok-p1*, *Thpok-p2*, *GATA3*, *Runx3*. Detected 4 h after RAPA (10 nM/20 nM) administration, n=3. (E) CD4(red), CD8(green) immunofluorescence in situ, scale bar = 100 μ m (100 ×). (F) Fluorescence intensity of Bcl-2/Bax in thymic non-subcapsular region, n=5. (H) *TRECs* level of mice, n=6.

3.1.4. Short-term RAPA decreases thymocyte telomere length and increases Sirt6 mRNA levels in thymus

To evaluate the effects of short-term RAPA treatment on thymic homeostasis, we examined thymic tissue and thymocytes(T. Wang et al., 2020). As shown in Fig. 3A, RAPA administration led to a reduction in thymocyte telomere length(Fig. 3A). Given the established roles of *Sirt3* and *Sirt6* as longevity-associated genes(J. Wang et al., 2020), we further assessed their expression levels. Our data revealed that RAPA markedly

upregulated *Sirt6* mRNA levels. Since p53 and p21 are well-characterized markers of cellular senescence, we analyzed their transcriptional responses to RAPA. Intriguingly, while RAPA significantly suppressed p53 mRNA levels in the thymus, it paradoxically affected p21 mRNA levels. Additionally, RAPA downregulated the mRNA levels of senescence-associated secretory phenotype (*SASP*) factors of IL- 1α (Fig. 3B). These findings suggest that short-term RAPA exposure induces thymic perturbations, potentially contributing to

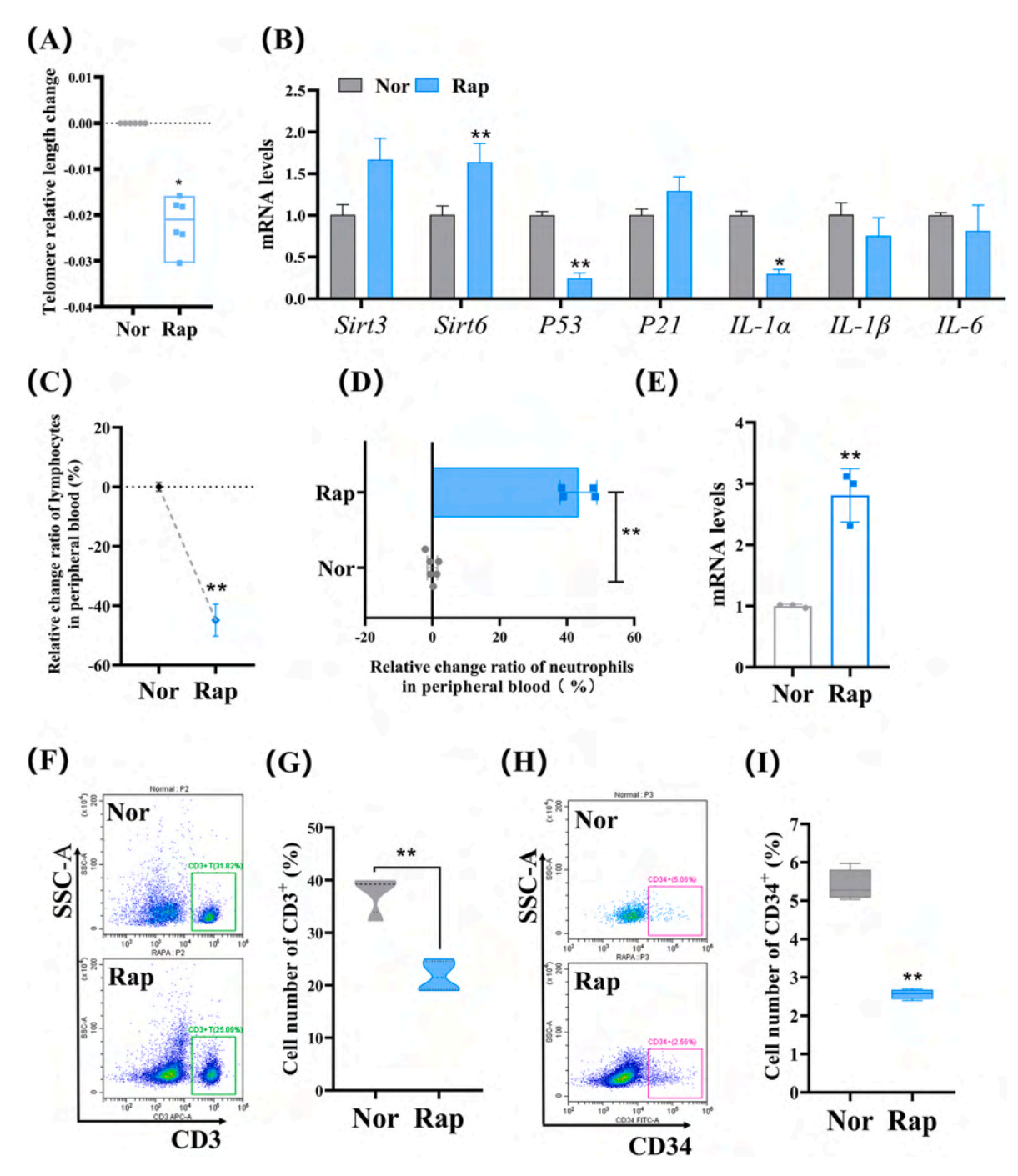


Fig. 3. Effects of short-term RAPA administration on gene and peripheral levels. (A) Changes in relative telomere length of thymocytes after short-term rapamycin administration, n = 6. (B) mRNA levels of *Sirt3*, *Sirt6*, *P53*, *P21* and *SASP*-related genes in thymus tissue, n = 6. (C) Relative change ratio of neutrophils detected in whole blood, n = 3. (D) Relative change ratio of lymphocytes detected in whole blood, n = 4. (E) mRNA levels of *CXCL12* in thymus, n = 3. (F–G) CD3⁺ T cells in peripheral blood were detected by flow cytometry, n = 3. (H–I) the ratio of CD34⁺ hematopoietic stem cells in peripheral blood were detected by flow cytometry, n = 3.

cellular senescence-related alterations.

3.1.5. Short-term RAPA lowers peripheral immune levels

Effective peripheral immunity is a critical prerequisite for successful T-cell reconstitution. RAPA exerts comprehensive regulatory effects on T-cell differentiation and development. Hematopoietic stem cells (HSCs) and neutrophils serve as key indicators of systemic immune competence. Biochemical analysis of whole blood revealed that RAPA treatment significantly increased the neutrophil population by approximately 43% (P < 0.01), while concurrently reducing the lymphocyte proportion by

about 45% (P < 0.01) (Fig. 3C and D). CXCL12, a chemokine known to mediate the migration of HSCs and neutrophils, was found to be upregulated in thymic tissue following RAPA administration(Bianchi et al., 2020). This elevated CXCL12 expression likely facilitates neutrophil recruitment to damaged thymic regions, potentially contributing to tissue regeneration (Fig. 3E). Notably, although RAPA maintained thymic output as evidenced by preserved *TRECs* level, peripheral blood analysis through either biochemical assays or flow cytometry demonstrated no proportional increase in lymphocytes(Fig. 3F and G). Given that CD34 $^+$ cell differentiation generates substantial T-cell precursors,

and considering clinical evidence that CD34 $^+$ depletion reduces thymic precursor influx(Benigni et al., 2016; Heitger et al., 1999), our observation of RAPA-induced peripheral CD34 $^+$ depletion suggests compromised T-cell regeneration capacity(P < 0.01). Taken together of these findings demonstrate that while RAPA suppresses peripheral lymphocyte-mediated immunity, the concomitant neutrophil expansion may provide compensatory supporting thymic repair processes.

3.2. Natural regeneration process of thymus after short-term RAPA administration

The thymus exhibits endogenous regenerative capacity poststimulation, with stromal niche alterations driving T cell reconstitution(Cosway et al., 2023). Following RAPA withdrawal, our longitudinal analysis at 3 and 14 days revealed distinct regenerative phases(Fig. 4A). Notably, thymus wet weight increased from 20.45 mg to 57.97 mg

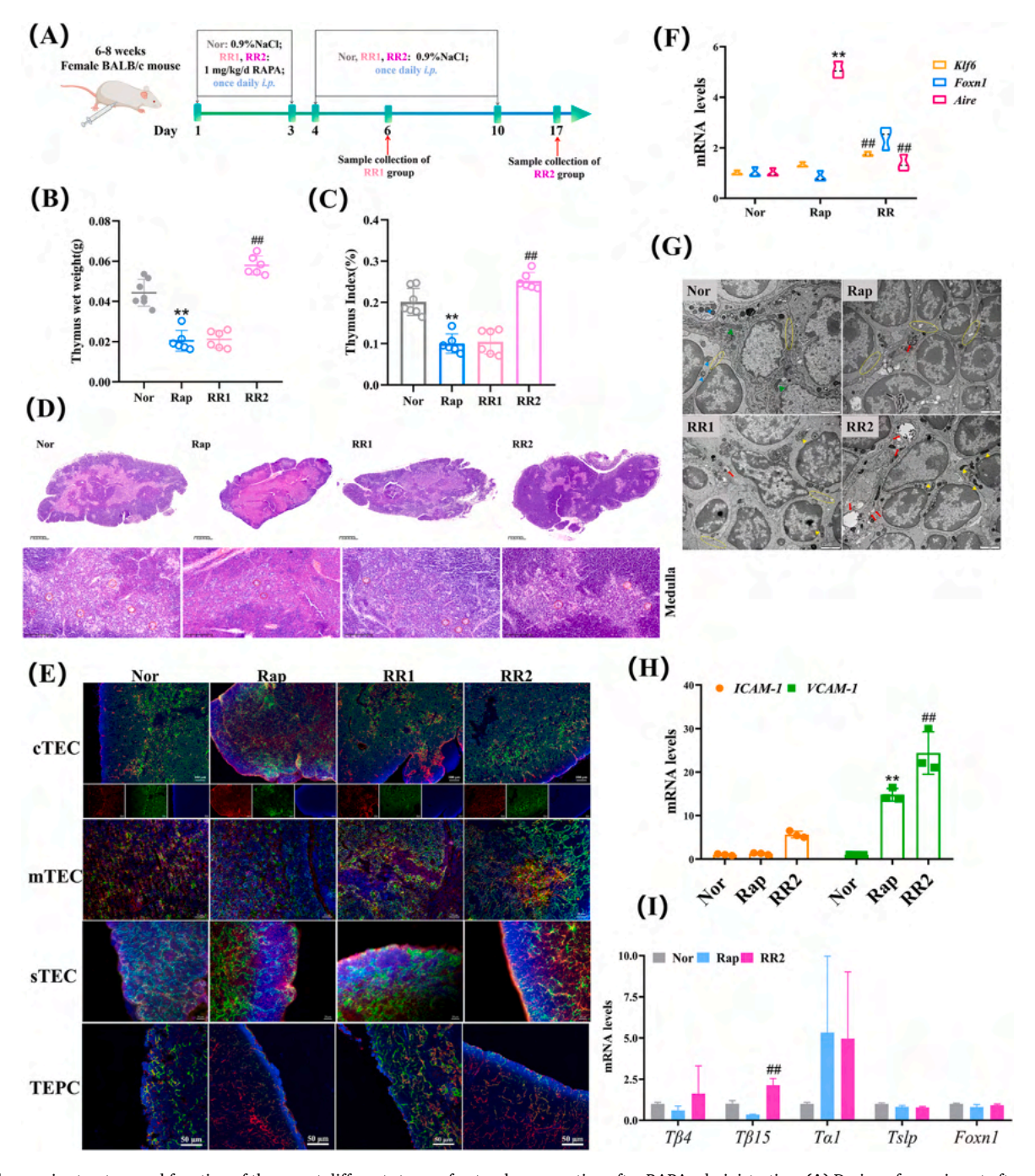


Fig. 4. Changes in structure and function of thymus at different stages of natural regeneration after RAPA administration. **(A)** Design of experiment after rapamycin withdrawal. **(B)** Thymus wet weight (g), n=6. **(C)** Thymus Index (%), n=6. **(D)** H&E staining pictures of thymic regeneration at different stages after RAPA administration. The scale bars were 625 μm(25 ×) and 200 μm(148 ×) respectively. Red circle represents the representative structure of epithelial cells wrapping thymocytes in the medulla. **(E)** Spatial distribution changes of TECs of thymus (CK5, red; CK8, green). cortex, scale bar = 100 μm. mTECs, scale bar = 50 μm. sTECs, scale bar = 20 μm. TEPCs, scale bar = 50 μm. **(F)** mRNA levels of *Klf6, Foxn1, Aire* genes related to iTEC function, n=6. **(G)** TEM observation of thymic ultrastructure, blue arrows represent normal mitochondria in thymocytes, green arrows represent normal mitochondria in stroma cells, yellow arrows represent aging mitochondria in thymocytes, yellow circles represent tight junctions between thymocytes, red arrows indicate autophagosomes, Scale bar = 2 μm. **(H)** mRNA levels of *ICAM-1* and *VCAM-1* in thymus, n=3. **(I)** mRNA levels of *Tβ4*, *Tβ15*, *Tα1*, *Tslp* and *Foxn1* in thymus, n=6.

(1.3-fold vs nor group) with concurrent thymus index elevation (P < 0.01) at day 14 (RR2 group)(Fig. 4B and C). These findings demonstrate that the change of thymic matrix microenvironment after RAPA withdrawal is the basis of thymus regeneration.

3.2.1. Thymic medulla remodeling and thymic volume enlargement in RAPA related natural regeneration

The thymus exhibited distinct stage-dependent histological alterations during RAPA-withdrawal regeneration. Compared to the Rap group, the RR1 group showed no significant change in thymus index. Conversely, the RR2 group displayed significant increases in both

thymic volume and index relative to the Rap group (P < 0.01), with thymus index exceeding Nor group by 25%. The H&E staining showed that RR1 group thymus had less distinct cortex-medullary boundaries than in Rap group, larger thymocyte gaps and thymocytes surrounded by mTECs was obvious (Fig. 4D, Supplementary Fig. 2C). But In RR2 group, thymus maintained a clearer cortex-medullary boundary, thymocytes arranged more closely in cortex and medulla, thymocyte increased significantly(P < 0.01), which was consistent with flow cytometry results (Supplementary Fig. 2D). And medulla distribution showed small area aggregation and multiple distribution characteristics. The recovery of thymus volume after RAPA administration provides an

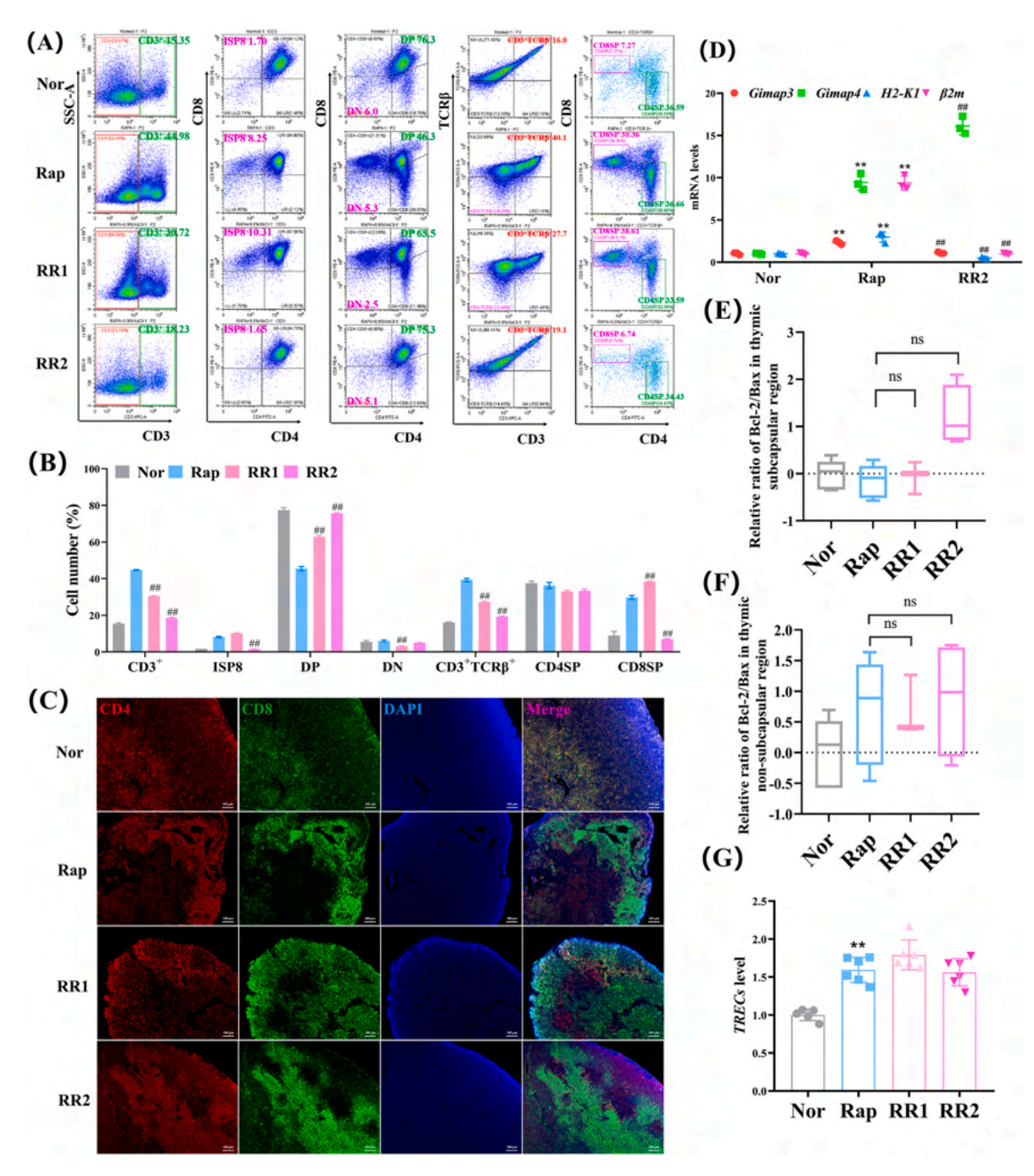


Fig. 5. Changes in T cell subsets at different stages of thymic regeneration after RAPA administration. **(A)** CD3⁺, CD3⁺TCRβ⁺, DP, DN, CD4SP, CD8SP, ISP8 of thymocytes were detected by flow cytometry, n = 3. **(B)** T cell subsets were counted by flow cytometry, n = 3. **(C)** CD4 (red), CD8 (green) double in situ fluorescence staining, scale bar = 100 μm(100 ×). **(D)** mRNA levels of positive selection *Gimap3*, *Gimap4*, *H2-K1*, $\beta 2m$ in thymus, n = 3. **(E)** Fluorescence quantitative analysis of Bcl-2/Bax in thymic subcapsular region, n = 3–6. **(G)** Detection of *TRECs* level in thymic output function, n = 6.

endogenous structural foundation for immune reconstitution.

3.2.2. sTECs expansion at day 3 and mTEC distribution widening at day 14 coincide with enhanced TEC function during regeneration

As core mediators of thymic regeneration, TECs orchestrate thymic microenvironments through thymosin secretion, establishing the foundation for thymocyte differentiation. During regenerative progression, CK5 expression exhibited stage-dependent upregulation compared to Rap group, with maximal induction during late-phase regeneration (RR2 group) coinciding with enhanced network structural organization (Fig. 4E). In the third image of Fig. 4E, while the capsule thickness remained unchanged in RR1, significant expansion occurred in RR2, the number of sTECs associated increased during regeneration. Biphenotypic CK5/CK8 epithelial clusters(In the forth image of Fig. 4E) emerged during early regeneration (RR1), with discrete co-localization patterns indicating thymic epithelial progenitor cells (TEPCs) involvement in the regeneration process. The number of thymocytes wrapped by each epithelial cell was more in RR2 group. In iTECs undergoing natural regeneration after RAPA induction, the mRNA levels of Klf6 and Foxn1 genes supporting TEC function was higher than that in Rap group, while Aire was lower than that in Rap group (Fig. 4F). TEM analysis demonstrated that with day 3 regeneration, specimens showed compact cellular organization compared to Rap group, while day 14 samples retained intercellular spacing despite enhanced stromal interactions (Fig. 4G). ICAM-1 mRNA levels post-regeneration indicated the maintenance of immune homeostasis(Fig. 4H). Notably, RAPA withdrawal triggered elevated $T\beta 4$, $T\beta 15$, and sustained $T\alpha 1$ mRNA levels versus the Nor group, although Foxn1 remained unchanged. Functional assays confirmed thymic functional restoration post-regeneration(Fig. 4I).

3.2.3. The positive selection (DP to CD8SP) is promoted at 3 days of regeneration, and the high ratio of CD3 $^+$ TCR β^+ T cell is maintained at 14 days of regeneration

Flow cytometry showed that the percentage of CD3⁺ T cells decreased significantly (P < 0.01) and maintained a higher level of T lymphocytes than normal at different stages of natural regeneration (Fig. 5A and B). In the regeneration process, the percentage of ISP8 T cells decreased from 10.3% to 1.65 %, but DP T cells recovered and the level increased significantly from 46.3% to 75.3% (P < 0.01). Compared with Rap group, DN T cells decreased by 52.8% (P < 0.01) at 3 days of regeneration. Thymus undergoing natural regeneration maintained a higher level of CD3⁺TCRβ⁺ T cells than normal thymus. Fig. 5B showed that the percentage of CD8SP T cells in the RR1 and RR2 groups was significantly lower than in the Rap group but higher than in the Nor group. RR2 group's percentage of CD8SP T cells decreased significantly than Rap group, and the level decreased to 6.74% (P < 0.01), which was about 7.3% lower than that in Nor group. DP T cells bound to MHC I molecules at an increased rate in RR1 group, which promotes the differentiation of DP T cells into CD8SP T cells, but this characteristic tends to be normal in RR2 group.

IF analysis revealed stage-specific spatial redistribution of CD8 expression, enriched within the subcapsular cortical region at 3 days regeneration, predominantly localized at the cortex-medullary junction at 14 days regeneration(Fig. 5C). By detecting genes related to positive selection, it was found that *Gimap4* mRNA levels increased, but *Gimap3*, H2-K1, $\beta 2m$ mRNA levels decreased after 14 days regeneration. H2-K1 and $\beta 2m$ are not only thymic positive selection-related genes, but also MHC I components, which explains the reduced proportion of CD8SP T cells in the flow results (Fig. 5D). In addition, there was no significant change in the level of thymus apoptosis and thymus output after 14 days regeneration (Fig. 5E–G).

3.2.4. Thymic p53 and p21 mRNA levels are decreased at 14 days of regeneration

To evaluate the functional integrity of thymic tissue following regenerative processes, we quantified relative telomere length in thymocytes. The results revealed significantly shortened relative telomere length in the RR1 group compared to Rap group, whereas RR2 maintained elongated telomeres(Fig. 6A). Sirt3 mRNA levels maintained normalizing post-regeneration, while Sirt6 remained elevated. Notably, P53 and P21 mRNA levels were maintained at lower level after thymic regeneration than Rap group(P < 0.01). The mRNA levels of SASP components IL-1 α , IL-1 β and IL-6 did not show significant changes. These molecular signatures collectively demonstrate robust preservation of thymic vitality following 14 days of regeneration, particularly in the RR2 group(Fig. 6B).

3.2.5. The percentage of CD34⁺ cells increases after natural regeneration

To assess peripheral immune reconstitution after endogenous thymus regeneration, we quantified key immune cell populations. Compared to the Rap group, the naturally regenerated group exhibited a statistically significant increase in the proportion of peripheral lymphocytes (P < 0.01) and a concomitant significant decrease in the ratio of neutrophils (P < 0.01) (Fig. 6C and D). CXCL12 mRNA levels approached baseline (Nor group) levels after 14 days of regeneration, and the levels were significantly lower than those in the Rap group (Fig. 6E). In addition, we found that the percentage of CD3⁺ T cells in peripheral blood decreased in RR1 group and maintained an increasing trend in RR2 group, but did not return to normal levels (Fig. 6F). Conversely, the percentage of CD34⁺ hematopoietic progenitor cells increased at various stages during thymic regeneration. Specifically, at 14 days post-regeneration, the CD34⁺ cell percentage was significantly elevated compared to the Nor group, representing an increase of approximately 20% (P < 0.05) (Fig. 6G).

3.3. IL-7 promotes immune function in thymic regeneration after RAPA administration

After acute thymic degeneration, some functions of thymus in natural regeneration process have not been completely restored. IL-7, an established thymopoietic cytokine, holds the potential to enhance thymic regeneration by driving T-cell proliferation and differentiation and maintaining thymic niche integrity through exogenous administration(Wang et al., 2022). So we explored the characteristics of its effect on thymus regeneration after RAPA withdrawal(Fig. 7A). In terms of thymus weight, IL-7 alone increased thymus index, but had no significant effect on thymus volume during regeneration after RAPA administration(Fig. 7B).

$3.3.1.\,$ IL-7 increases the number of thymocytes and the spatial distribution of cTEC at 3 days of regeneration

IL-7 administration did not significantly affect thymic wet weight or index versus natural regeneration, though RI1 showed 7.7 % increase over RR1 (Fig. 7C). H&E staining revealed minimal IL-7 impact on cortex-medullary distribution early in regeneration. Later (RI2), IL-7 enhanced cortical cellularity and promoted medullary epithelial encapsulation of thymocytes (Fig. 7D), with significantly increased thymocyte numbers (Supplementary Fig. 2E and F). cTEC spatial expression was broader in RI1 vs RR1, but similar in RI2 and RR2 (Fig. 7E). IL-7 promoted stellate cTECs development, enriching thymocyte encapsulation. Enhanced stellate sTECs occurred in both RI1 and RI2. RI2 exhibited stromal adaptations, increased capsular thickness and capsular zone CK8 expression vs RR2, suggesting IL-7 orchestrates niche remodeling via thymocyte proliferation and cortical stromal reinforcement. In vitro, IL-7 selectively upregulated Foxn1 mRNA levels versus RR group and significantly reduced thymic VCAM-1 mRNA levels during regeneration (Fig. 7F and G). Ultrastructurally, day 3 post-regeneration thymocytes displayed tight junctions and stromal cells contained increased autophagosomes in both RI1 and RR1, though these differences were transient (Fig. 7H). RI2 showed IL-7-induced elevation of Tslp and Foxn1 mRNA but significant reduction of $T\beta$ 15 (P < 0.01) vs RR2 (Fig. 7I).

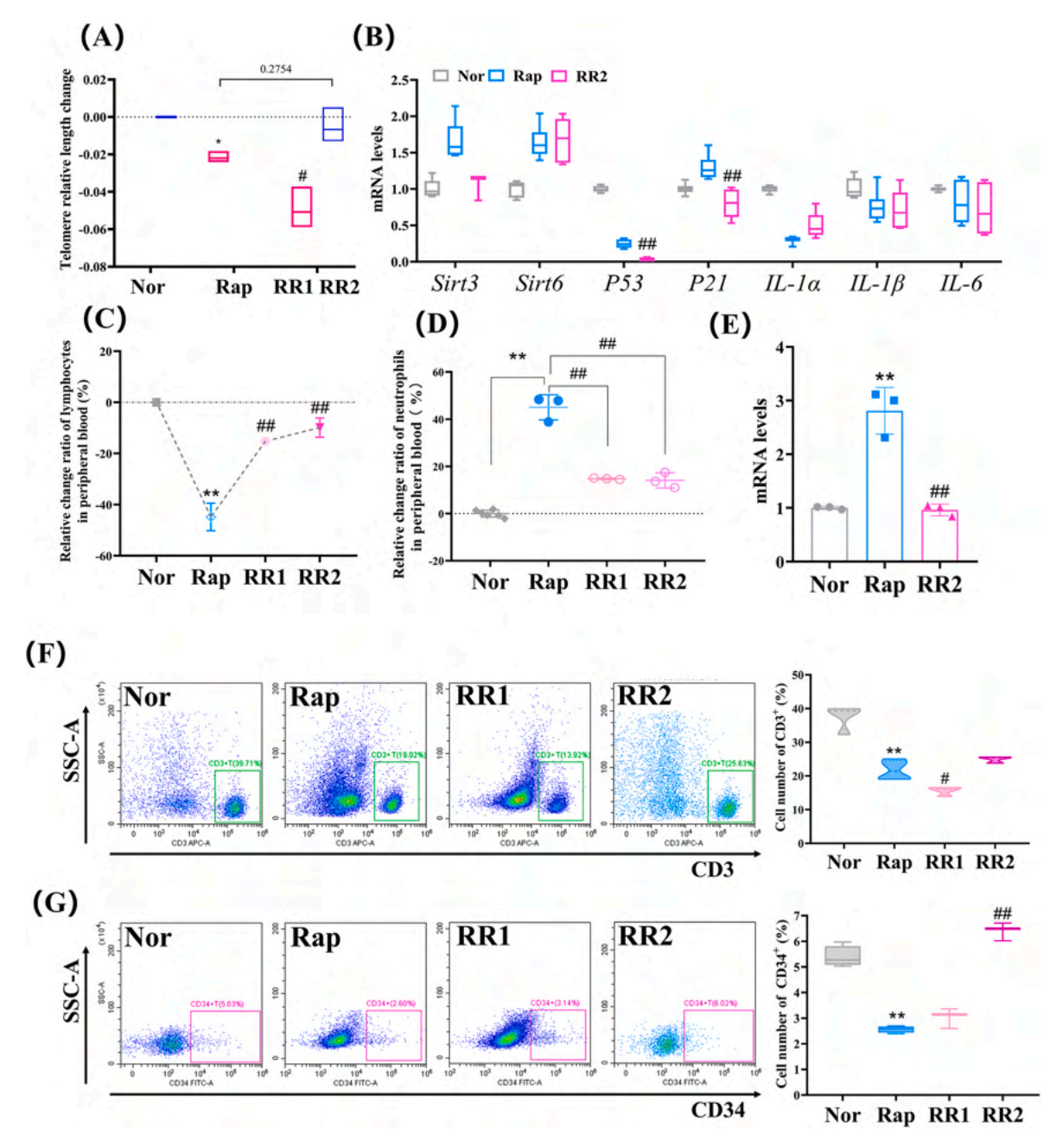


Fig. 6. Changes of mRNA and peripheral immune level in different stages of thymic endogenous regeneration. **(A)** Changes of relative telomere length of thymocytes, n = 3. **(B)** mRNA levels of *Sirt3*, *Sirt6*, *P53*, *P21* and *SASP*-related genes in thymus tissue, n = 6. **(C)** Relative change ratio of neutrophils detected in whole blood, n = 3. **(D)** Relative change ratio of lymphocytes detected in whole blood, n = 3. **(E)** mRNA levels of *CXCL12* in thymus, n = 3. **(F)** CD3⁺ T cells in peripheral blood were detected by flow cytometry, n = 3. **(G)** the ratio of CD34⁺ hematopoietic stem cells in peripheral blood were detected by flow cytometry, n = 3.

3.3.2. IL-7 maintains H2-K1 and β 2m high mRNA levels at 14 days of regeneration

IL-7 significantly modulates T cell subset dynamics and maturation during thymic regeneration. Flow cytometry revealed that IL-7 administration reduced the proportion of CD3 $^+$ T cells in the thymus of RI1 group mice from 30.5% to 26.7%, while this proportion increased in the RI2 group. Further analysis of T cell maturation demonstrated stage-specific effects, IL-7 could promote the selection of DP T cells towards CD4SP T cells during the regeneration of RI1. Conversely, in regeneration of RI2, IL-7 significantly elevated the CD8SP T cells proportion (7.0%–10.7%, P < 0.01)(Fig. 8A and B). IF corroborated these findings, showing sustained CD4 expression intensity in RI1 compared to RR1. However, the characteristic subcapsular cortical concentration of CD8-high regions observed in RR1 was absent in RI1 and lost entirely in

RI2 (Fig. 8C).

IL-7 regulated key genes involved in thymocyte differentiation. Treatment downregulated *Gimap4* mRNA and upregulated exogenous H2-K1 and $\beta 2m$ mRNA levels in the RR2 group (Fig. 8D). Furthermore, both low (0.05 µg) and high (0.5 µg) dose IL-7 elevated *Thpok* and *GATA3* mRNA levels, indicating a propensity towards CD4SP lineage commitment. This aligns with the increased CD4SP T cells proportion observed in RI1. This pro-CD4 effect was transient, not sustained in later regeneration (RR2). Conversely, elevated expression of MHC class I molecules H2-K1 and $\beta 2m$ in RR2 revealed IL-7's role in promoting DP selection towards the CD8SP lineage at this stage (Fig. 8E). Also, the results showed that IL-7 exhibited region-specific apoptotic regulation in the thymus. Early IL-7 administration significantly enhanced antiapoptotic activity in the subcapsular region, although this effect was

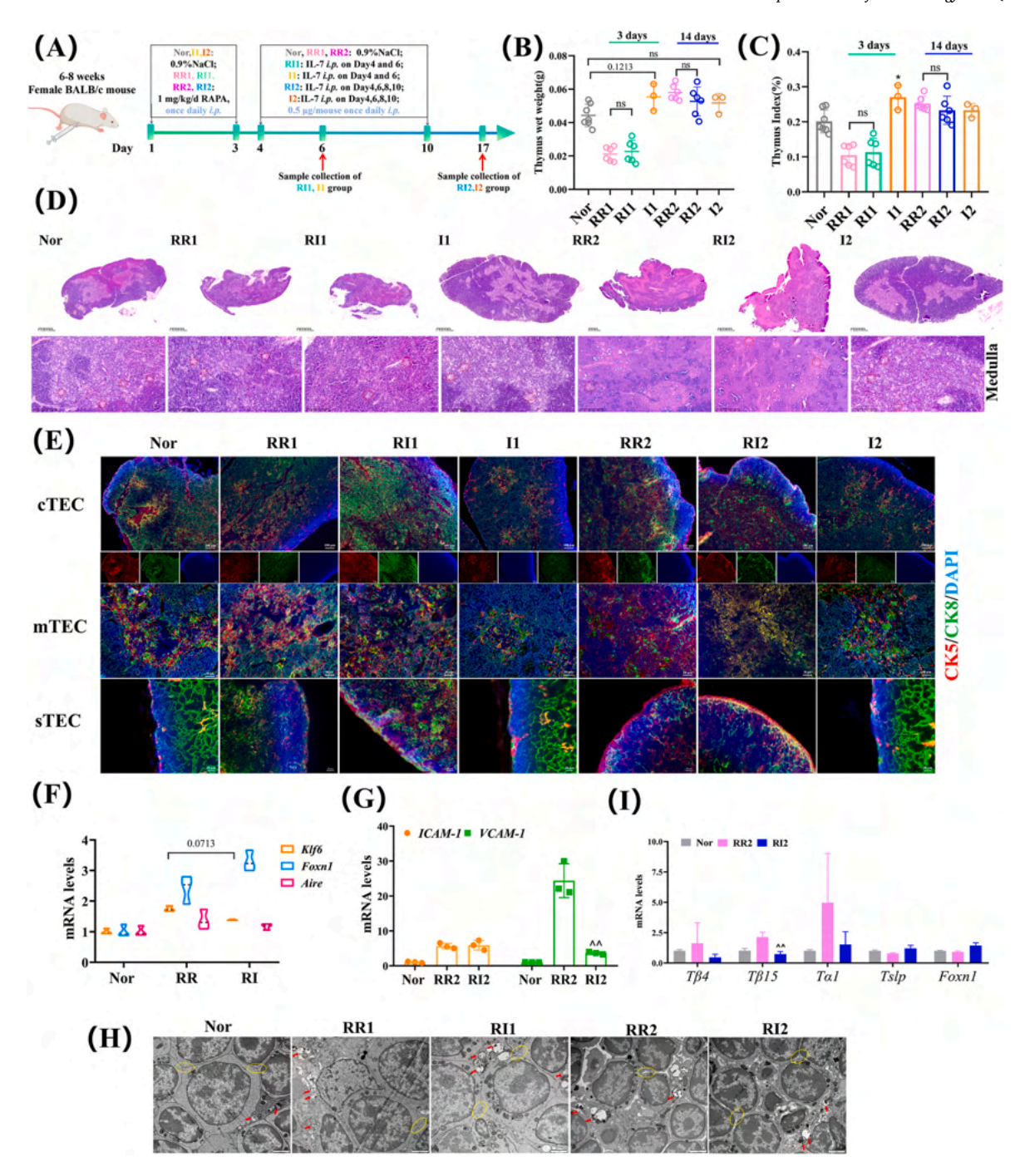


Fig. 7. Effect of IL-7 on the structure and function of thymus during natural regeneration of thymus. **(A)** Experimental design of IL-7 administration after rapamycin withdrawal. **(B)** Thymus wet weight (g), n = 3–7. **(C)** Thymus Index (%), n = 3–7. **(D)** H&E staining of thymus. The scale bars were 625 μm(25 ×) and 200 μm(148 ×) respectively. Red circle represents the representative structure of epithelial cells wrapping thymocytes in the medulla. **(E)** Spatial distribution changes of TECs of thymus (CK5, red; CK8, green). cTECs, scale bar = 100 μm. mTECs, scale bar = 50 μm. sTECs, scale bar = 20 μm. **(F)** mRNA levels of function-related genes *Klf6*, *Foxn1* and *Aire* in iTECs were detected, n = 3. **(G)** mRNA levels of *ICAM-1* and *VCAM-1* in thymus, n = 3. **(H)** TEM observation of thymus ultrastructure, attention to tight junctions between thymocytes, red arrows pointing to mitochondrial autophagy, scale bar = 2 μm. **(I)** mRNA levels of thymosin-related genes $T\beta 4$, $T\beta 15$, $T\alpha 1$, Tslp and Tslp and Tslp in thymus, Tslp in thymu

not maintained in later regeneration (Fig. 8F). In non-subcapsular regions, IL-7 failed to augment the anti-apoptotic effect induced by RAPA alone (Fig. 8G). Critically, IL-7 enhanced TRECs level during early regeneration (P < 0.05) (Fig. 8H). These data demonstrate that IL-7 exerts a dual function in thymic regeneration, modulating T cell maturation quality control and augmenting thymic output and mediated through region-specific apoptosis regulation.

3.3.3. IL-7 prolongs the telomere length of thymocytes and maintains higher mRNA levels of Sirt3 and P21

While IL-7's thymopoietic benefits are well-documented, its impacts on thymic post-RAPA treatment remained unexplored. The results revealed IL-7 administration elongated thymocyte telomeres in both RR1 and RR2 group vs Rap group (Fig. 9A). Fig. 9B analysis demonstrated superior thymic Sirt3 maintenance with IL-7 vs RR2 group (P < 0.01). Although not enhancing Sirt6 mRNA levels, IL-7-treated groups sustained higher Sirt6 mRNA levels than Nor group. The results also

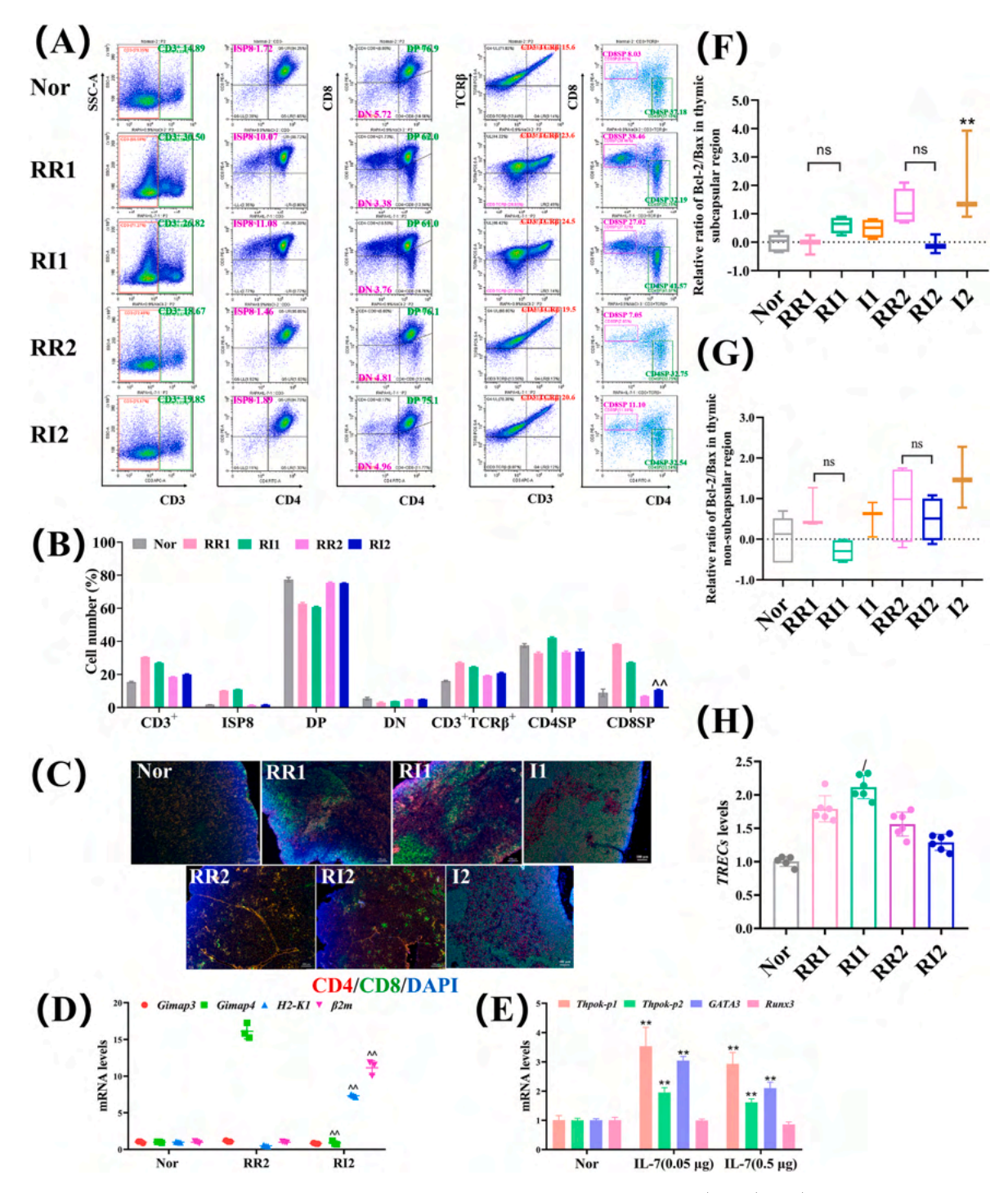


Fig. 8. Effects of IL-7 application during natural regeneration on the distribution of T cell subsets. **(A)** CD3⁺, CD3⁺TCRβ⁺, DP, DN, CD4SP, CD8SP, ISP8 of thymocytes were detected by flow cytometry. **(B)** T cell subsets were counted by flow cytometry, n = 3. **(C)** CD4 (red), CD8 (green) immunofluorescence staining in situ, scale bar = $100 \, \mu m(100 \times)$. **(D)** mRNA levels of positive selection *Gimap3*, *Gimap4*, *H2-K1*, $\beta 2m$ in thymus, n = 3. **(E)** 4 h after IL-7 administration, mRNA levels of negative selection *Thpok-p1*, *Thpok-p2*, *GATA3*, *Runx3* in thymocytes, n = 3. **(F)** Fluorescence quantitative analysis of Bcl-2/Bax in thymic subcapsular region, n = 3-6. **(H)** Detection of *TRECs* level in thymic output function, n = 6.

showed that IL-7 significantly increased P21 mRNA levels (P<0.01). Notably, IL-6, $IL-1\alpha$ and $IL-1\beta$ were not significantly different in RI2 group compared with RR2 group. These findings explain the potential reasons of IL-7's regenerative capacity, telomere preservation through Sirt3 mediated mechanisms and senescence mitigation via uncoupled regulation of P53/P21 and inflammatory pathways.

3.3.4. IL-7 enhances peripheral immune reconstitution without altering ${\it CD34}^+$ cell proportions

Thymic natural regeneration post-rapamycin withdrawal establishes a foundation for immune recovery. IL-7 exhibited time-dependent therapeutic effects during this process. By day 14, RI2 demonstrated significantly improved lymphocyte proportions ν s RR2 (P < 0.01), restoring levels to baseline (Fig. 9C). A parallel restoration occurred in neutrophils (P < 0.01) (Fig. 9D). Notably, *CXCL12* mRNA levels remained unaltered between RI2 and RR2 (Fig. 9E). Flow cytometry

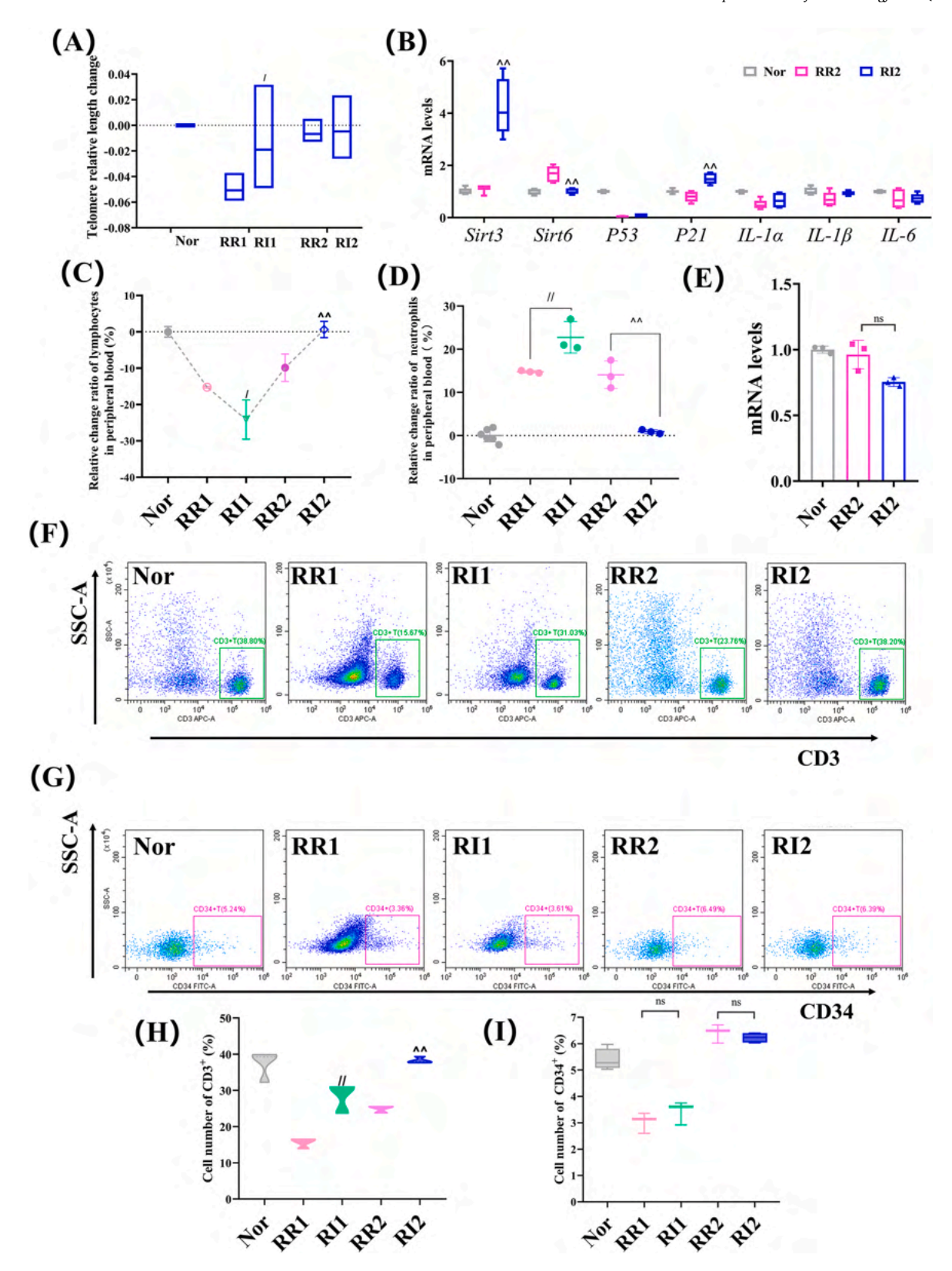


Fig. 9. IL-7 promotes peripheral immune recovery and increases *Sirt3* and *P2*1 mRNA levels. (**A**) Changes in relative telomere length of thymocytes, n = 3. (**B**) mRNA levels of *Sirt3*, *Sirt6*, *P53*, *P21* and *SASP*-related genes in thymus tissue, n = 6. (**C**) Relative change ratio of neutrophils detected in whole blood, n = 3. (**D**) Relative change ratio of lymphocytes detected in whole blood, n = 3. (**E**, **H**) mRNA levels of *CXCL12* in thymus, n = 3. (**F**) CD3⁺ T cells in peripheral blood were detected by flow cytometry, n = 3. (**G**, **I**) Detection of CD34⁺ hematopoietic stem cells in peripheral blood by flow cytometry, n = 3.

revealed IL-7 significantly elevated CD3 $^+$ T cell percentages in both RI1 and RI2 groups(P < 0.01) (Fig. 9F and H). Crucially, IL-7 exerted no regulatory effect on CD34 $^+$ cells, proportions persisted at 3.43% in RI1 and 6.23% in RI2 groups(Fig. 9G and I).

3.4. MET enhances immune function remodeling after RAPA administration

As a recognized anti-aging drug, MET enhances thymic architecture and modulates immune function through mitochondrial optimization and autophagy induction(Reis et al., 2023; Xie et al., 2021; Yang et al., 2022). After RAPA administration, the use of MET enhanced immune profiles, evidenced by RMH2 group's thymus wet weight (58.53 mg) and

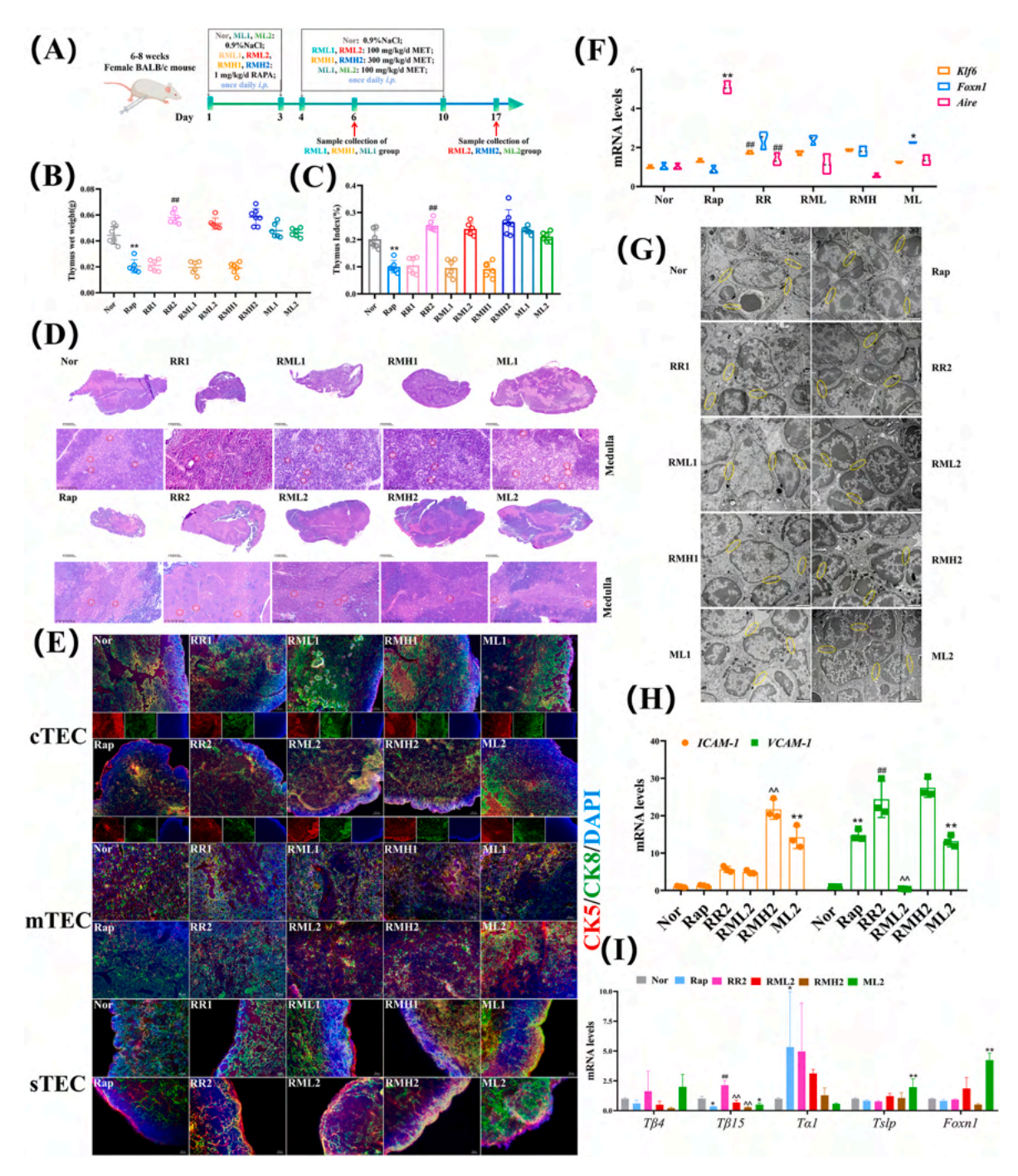


Fig. 10. Effects of MET application during natural regeneration on thymic structure and function. **(A)** Experimental design of MET administration after rapamycin withdrawal. **(B)** Thymus wet weight (g), n = 6–7. **(C)** Thymus Index (%), n = 6–7. **(D)** H&E staining of thymus. The scale bars were 625 μm(25 ×) and 200 μm(148 ×) respectively. Red circle represents the representative structure of epithelial cells wrapping thymocytes in the medulla. **(E)** Spatial distribution changes of TECs of thymus (CK5, red; CK8, green). cTECs, scale bar = 100 μm. mTECs, scale bar = 50 μm. sTECs, scale bar = 20 μm. **(F)** RML or RMH group (24 h after RAPA administration, MET (0.1 μM administration) was replaced for 24 h), ML group (24 h after normal medium culture, MET (0.1 μM administration) was replaced for 24 h), mRNA levels of *Klf6, Foxn1*, *Aire* genes related to iTEC function, n = 6. **(G)** TEM observation of thymus ultrastructure, yellow circles represent thymocyte tight junction structure. **(H)** mRNA levels of *ICAM-1* and *VCAM-1* in thymus, n = 3. (I) mRNA levels of $T\beta4$, $T\beta15$, Ta1, Ts1p and Foxn1 in thymus, n = 6.

thymus index (0.265%) (Fig. 10A–C). This demonstrates unique thymopoietic dynamics distinct from monotherapy approaches of RAPA, suggesting MET's multi-modal action integrates metabolic reprogramming with stromal remodeling.

3.4.1. MET decreases the number of thymocytes and $T\beta15$ mRNA levels after natural regeneration

Application of MET during natural regeneration revealed several key features of thymic structural restoration. H&E staining indicated that while the cortex-medullary architecture remained disorder in the RML1 and RMH1 groups, a significant reduction in thymocyte density was

observed, particularly within disorganized medullary regions where epithelial cell-surrounded thymocytes were diminished (Fig. 10D). Conversely, MET administration had no significant effect on the distribution of thymic cortex-medullary structure, and the RMH2 group maintained a better cortex-medullary boundary. Notably, the METL2 group exhibited a more pronounced structural feature where medullary epithelial cell clusters tightly enveloped thymocytes. Furthermore, MET treatment significantly reduced total thymocyte numbers compared to the RR2 group, an effect more pronounced in the RML2 group (Supplementary Fig. 2G).

MET application influenced both the quantity and spatial

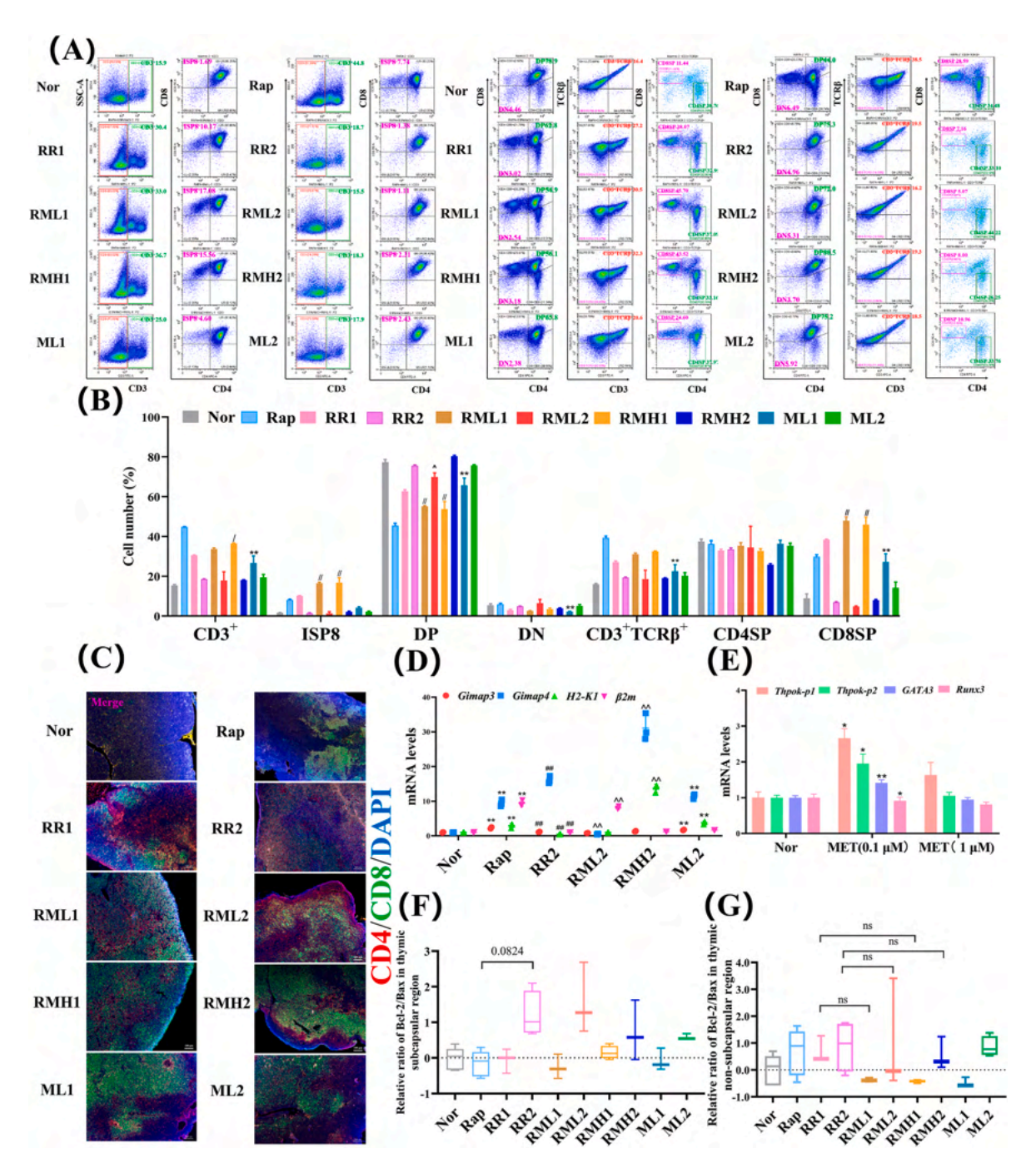


Fig. 11. Effects of MET on T cell subsets during natural regeneration. (A) Flow cytometry analysis of thymocyte CD3⁺, CD3⁺TCRβ⁺, DP, DN, CD4SP, CD8SP, ISP8 grouping diagram. (B) Flow cytometry was used to detect thymocyte index, n = 3. (C) CD4 (red), CD8 (green) double fluorescence staining in situ, scale 100 μm(100 ×). (D) mRNA levels of positive selection *Gimap3*, *Gimap4*, *H2-K1*, β2m in thymus, n = 3. (E) 4 h after MET(0.1 μM/1 μM) administration, mRNA levels of negative selection genes *Thpok-p1*, *Thpok-p2*, *GATA3*, *Runx3* in thymocytes, n = 3. (F) Fluorescence quantitative analysis of Bcl-2/Bax in subcapsular cortex of thymus tissue, n = 3–6.

distribution of TECs. In the RML1 and RMH1 groups, cTECs displayed a predominant increase in distribution. However, in the RML2 and RMH2 groups, cTECs no longer occupied broader regions; instead, mTECs exhibited expanded spatial distribution (Fig. 10E). Our results indicate a temporal shift in MET's primary effect, transitioning from an initial influence on cTECs to a predominant impact on medullary TECs at later stages. This shift correlated with increased numbers of mTEC-enveloped thymocytes and medullary reticular epithelial cells in the RML2 and RMH2 groups. This spatial redistribution was time-dependent, characterized by sTEC loss and capsular thickening at day 3, as evidenced by enriched subcapsular CK8 expression at day 14.

During natural regeneration, MET did not significantly elevate mRNA levels of *Klf6* or *Foxn1* in TECs, consistent with prior findings(Xie et al., 2021) (Fig. 10F). Specifically, MET promoted the formation of tight junctions and increased desmosome numbers in the RML2 and RMH2 groups, effects not observed in the RML1 and RMH1 groups (Fig. 10G). MET also sustained higher mRNA levels of *ICAM-1* and *VCAM-1* after regeneration, suggesting enhanced intercellular adhesion potentially affecting thymic output function (Fig. 10H). Additionally, MET exerted significant effects primarily on *Tslp* and $T\beta15$. Combined with observed increases in *Foxn1* mRNA levels, these data indicate that the RML2 group sustains a higher regenerative state in the thymus (Fig. 10I).

3.4.2. MET regulates T cell subsets in the regenerative phase in a dose- and time- dependent manner

Flow cytometric analysis (Fig. 11A and B) revealed significant alterations in thymocyte subsets following MET intervention. Compared to the Nor group, the ML1 group exhibited an elevated proportion of ISP8 T cells. Concomitantly, DP T cells were markedly reduced to 62.8% (P < 0.01), DN T cells decreased to 2.3% (P < 0.01), while CD3⁺TCR β ⁺ T cells increased to 22.6% (P < 0.01) and CD8SP T cells rose to 27.3% (P< 0.01). Relative to the RR1 group, the RMH1 group demonstrated significantly higher proportions of CD3 $^+$ T cells (P < 0.05) and ISP8 T cells (P < 0.01). Notably, early MET administration (RML1/RMH1) increased ISP8 T cells by 61.5%-65.2% and CD8SP T cells by 19.7%-24.7% (P < 0.01). However, the sustained impact of MET on regeneration was not maintained; compared to RR2, the RML2 group showed a significant reduction in DP T cells (P < 0.05). These dynamic shifts suggest that MET promotes T cell maturation at day 3 post-regeneration, potentially by stage-dependently modulating DP T cells differentiation to preferentially drive commitment towards the CD8⁺ lineage.

IF analysis of CD4/CD8 distribution uncovered distinct spatial patterns associated with MET intervention. Compared to Nor group, both ML1 and ML2 groups displayed increased proportions of CD8⁺ T cells, forming high-density clusters predominantly in the cortex-medulla regions. Enhanced CD8⁺ T cell infiltration in the subcapsular zone was observed in RML1 compared to RR1, resembling the pattern seen in RMH1. RML2 exhibited elevated proportions of both CD4⁺ and CD8⁺ T cells, characterized by prominent CD4⁺ T cell aggregation conversely. In contrast, RMH2 showed dispersed CD8+ T cells exceeding RR2 levels (Fig. 11C). RML2 group was able to significantly reduce the Gimap4 mRNA levels, and in RMH2 group, the mRNA levels of Gimap4 and H2-K1 were significantly increased (P < 0.01) (Fig. 11D). In vitro studies demonstrated MET-induced dose-dependent modulation of negative selection markers, with Thpok and GATA3 mRNA levels increasing proportionally while Runx3 decreased inversely (Fig. 11E). Higher MET doses corresponded with a weaker propensity for CD4SP lineage commitment, accompanied by a decreasing trend in Runx3 mRNA levels. Analysis of apoptosis revealed regional specificity (Fig. 11F and G). The thymic subcapsular zone exhibited MET-insensitive anti-apoptotic activity. In contrast, the non-subcapsular regions displayed MET-mediated pro-apoptotic effects, particularly prominent during the early regeneration phase. Results demonstrate that MET orchestrates thymocyte kinetics through dose and time dependent mechanisms. This involves coordinated regulation of surface markers, transcriptional regulators (Thpok, GATA3, Runx3), and region-specific modulation of apoptotic pathways.

3.4.3. MET increases Sirt3 but decreases Sirt6 mRNA levels

As illustrated in Fig. 12A, MET administration significantly enhanced *TRECs* level, with particularly pronounced effects observed at a low dose (P < 0.01), suggesting improved thymic output functionality. Quantitative analysis of thymocyte relative telomere length revealed MET's potential telomere-prolonging capacity (Fig. 12B). mRNA levels in Fig. 12C demonstrated elevated mRNA levels of *P53*, *P21*, and *IL-1* α in the ML2 group (Fig. 12C). Comparative analysis of sirtuin expression revealed that RML2 maintained significantly higher *Sirt3* mRNA levels than both RMH2 and RR2 groups, while *Sirt6* mRNA levels showed the similar elevation relative to RMH2. Although both RML2 and RMH2 groups comparably suppressed *P53* mRNA levels, RML2 exhibited markedly elevated *IL-1* α mRNA levels compared to RR2 group.

3.4.4. MET promotes peripheral immunity and increases the ratio of CD3⁺

To evaluate MET's impact on peripheral immunity during post-RAPA thymic regeneration, we conducted multi-parametric analyses. MET showed negligible effects on peripheral blood lymphocyte proportions vs Nor group (Fig. 12D). Neutrophils dynamics remained stable across MET-treated groups, with RML2/RMH2 exhibiting marginally reduced fluctuations versus RR2 group (Fig. 12E). In MET-treated thymus tissue, we detected a significant increase in CXCL12 mRNA levels, and higher mRNA levels were observed in groups RML2 and RMH2 than in RR2 group (Fig. 12F). However, CD3⁺ T cells in peripheral blood and found different results from whole blood lymphocyte detection. For example, MET alone significantly reduced the ratio of CD3 $^+$ T cells (P < 0.01). RML1 group and RMH1 group significantly increased the ratio of CD3⁺ T cells compared with RR1 group (P < 0.01), and RML2 group established better immune levels than normal at 14 days (Fig. 13A and C). In addition, MET administration for only 3 days directly resulted in a significant reduction in the ratio of CD34⁺ cells, whereas higher CD34⁺ levels were found in ML2 group (P < 0.01) (Fig. 13B and D). Phasespecific modulation of CD34⁺ populations by post-RAPA MET administration suggests enhanced T cell reconstitution potential.

4. Discussion

Building upon current thymic regeneration models, our study delineates acute thymic involution and recovery induced by short-term low-dose RAPA through three distinct phases, degeneration, progressive disorganization, and reconstruction. RAPA administration disrupted corticomedullary demarcation, manifesting as increased capsular thickness and concomitant loss of sTECs and reticular mTECs. These observations align with reported reductions in mTEC proportions following TEC-specific mTOR deletion(Liang et al., 2018). As an mTOR inhibitor, RAPA's detrimental impact on thymic medullary architecture corroborates H&E results. Critically, the depletion of CD34⁺ hematopoietic progenitors (coupled with sTECs loss) likely impedes the differentiation of ETPs into DN T cells within the subcapsular niche(Nitta et al., 2021). This mechanistic disruption collectively impedes DN-to-DP T cell transition, providing a plausible explanation for DN thymocyte accumulation during RAPA-induced involution.

Compartment-specific functions govern thymocyte development, the cortex facilitates positive selection, whereas the medulla mediates negative selection(Tong et al., 2024). RAPA treatment upregulated key positive selection regulators (Gimap3, Gimap4, H2-K1, $\beta 2m$). As MHC class I components, H2-K1 and $\beta 2m$ preferentially promote CD8SP T cell commitment. We posit that diminished anti-apoptotic activity in non-subcapsular zones, where DP T cells engage MHC-I complexes on TECs, provides a mechanistic basis for elevated CD8SP T cells proportions. This aligns with reduced MHC-II⁺ TECs in TEC-specific mTOR^{CKO} models, indicating RAPA modulates MHC-I/II balance

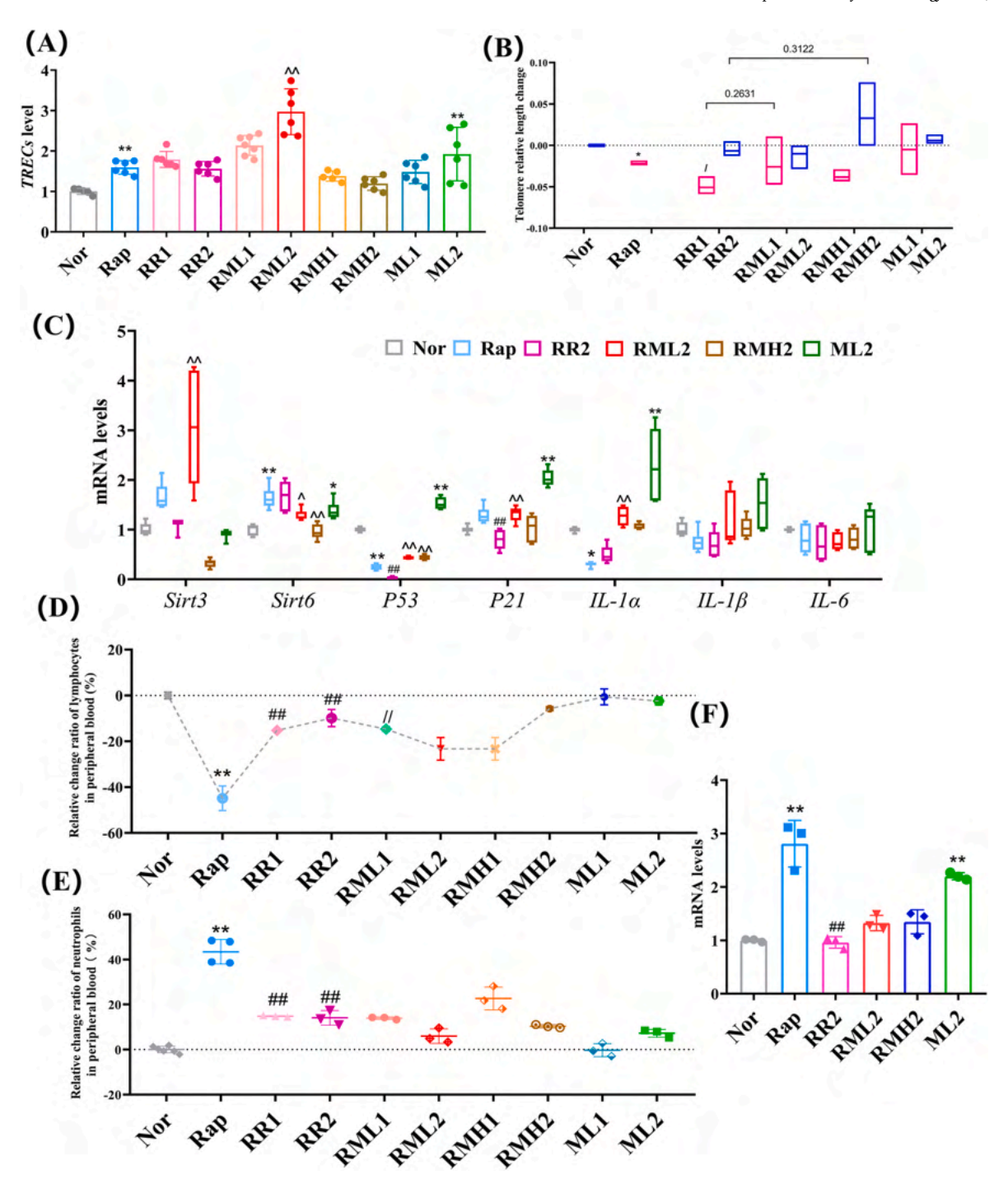


Fig. 12. MET increased *TRECs* level and *Sirt3* mRNA levels. **(A)** Detection of *TRECs* level in thymic output function, n = 6. **(B)** Changes of relative telomere length of thymocytes, n = 3. **(C)** mRNA levels of *Sirt3*, *Sirt6*, *P53*, *P21* and *SASP*-related genes in thymus tissue, n = 6. **(D)** Relative change ratio of lymphocytes detected in whole blood, n = 3. **(E)** Relative change ratio of neutrophils detected in whole blood, n = 3. **(F)** mRNA levels of *CXCL12* in thymus, n = 3.

(Damoiseaux et al., 1996; Elyahu and Monsonego, 2021). Concomitant $\mathit{Klf6}$ upregulation supports thymic function, while enhanced Aire mRNA levels in mTECs reinforces thymocyte adhesion and negative selection (Lopes et al., 2022). Nonlinear $\mathit{P53/P21}$ interactions implicate cell cycle dysregulation in RAPA-mediated telomere attrition (Graf et al., 2017; Hill et al., 2024; Lesniewski et al., 2017). Increased $\mathit{Sirt6}$ mRNA levels reflects RAPA's anti-senescence properties. Crucially, RAPA-induced thymic involution correlates with altered thymosin profiles, elevated $\mathit{Ta1}$ and modified $\mathit{Tβ15}$ mRNA levels may counteract $\mathit{Ta1}$'s established role in CD4⁺ T cell and TRECs reconstitution, positioning them as potential mediators of RAPA-driven thymic degeneration(Chen et al.,

2024; Liu et al., 2020; Tong et al., 2020).

The thymus undergoes endogenous regeneration following environmental or pharmacological stimuli, wherein stromal remodeling mediates T cell reconstitution(Sharma et al., 2021). Short-term low-dose RAPA similarly triggers this intrinsic regenerative program, and RAPA's immunomodulatory effects exhibit a "memory" phenotype, By day 3 post-cessation, positive selection remained biased toward MHC class I engagement, sustaining elevated CD8SP T cells proportions despite increased DP T cells relative to Rap groups. This persistence aligns with reports that RAPA promotes tissue-resident memory CD8+ T cells through metabolic reprogramming (reduced glycolysis/increased fatty

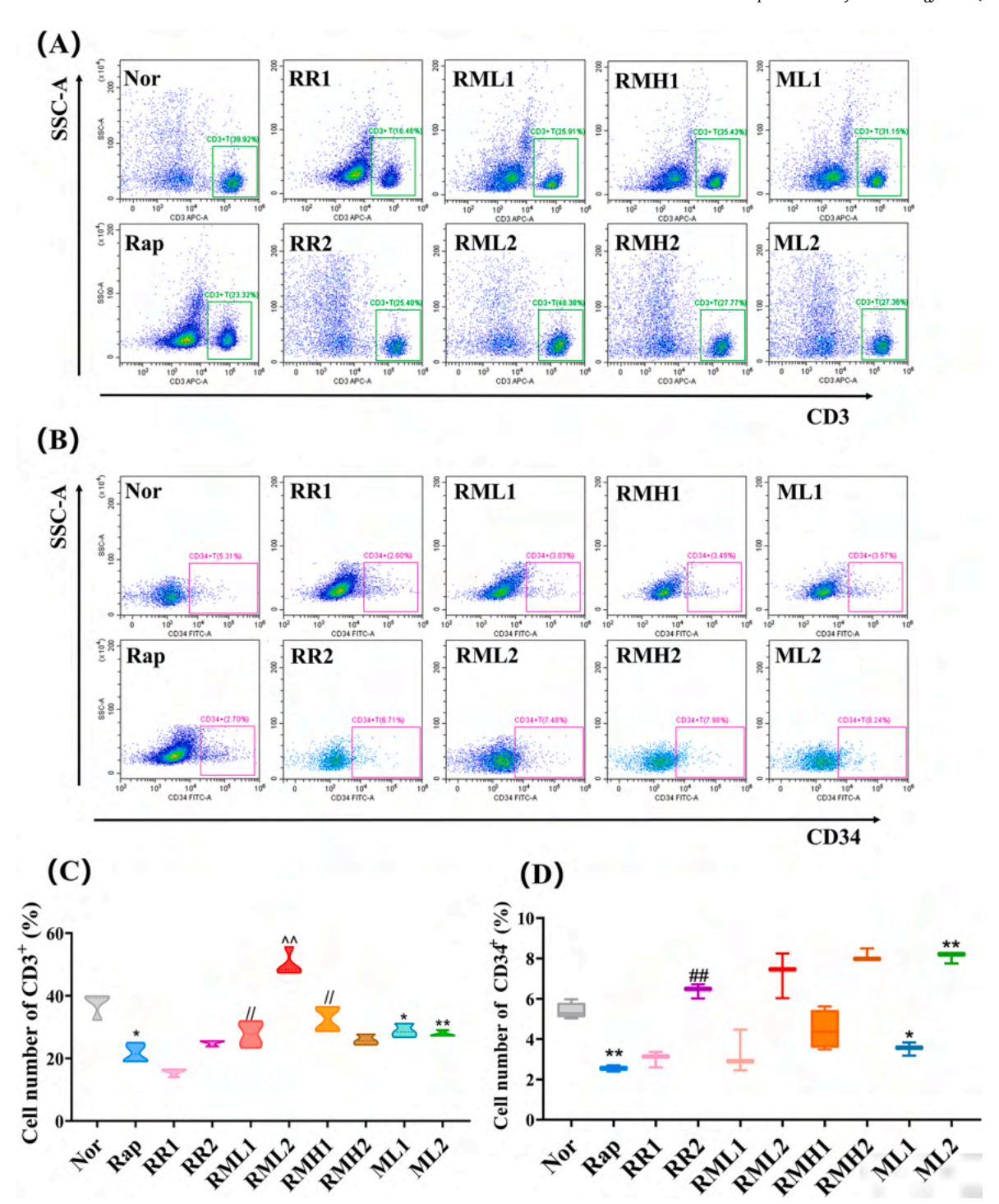


Fig. 13. Effects of MET on peripheral CD3⁺ T cells and CD34⁺ cells during natural regeneration. **(A, C)** CD3⁺ T cells in peripheral blood detected by flow cytometry. **(B, D)** CD34⁺ hematopoietic stem cells in peripheral blood were detected by flow cytometry, n = 3.

acid oxidation), thereby facilitating regenarated thymic (Xiao ML et al., 2019). CD4SP suppression persisted at both day 3 and 14 without normalization. These findings demonstrate RAPA's dual regulation of positive/negative selection – mechanistically corroborated by Raphael et al.(Barros et al., 2024) – wherein sustained MHC-I bias and unresolved CD4SP deficiency collectively shape post-regenerative T cell homeostasis.

Furthermore, spatial reduction of CK8 expression was observed at 14 days post-natural regeneration, particularly within subcapsular epithelial-deficient zones. Critically, thymoproteasomes containing the catalytic subunit β 5t (Psmb11) in cTECs generate unique peptide motifs

essential for positive selection of CD8 $^+$ T cells. SP T cells undergo apoptosis upon failure to recognize or strong binding to MHC molecules (Takaba et al., 2017). While subcapsular and cortical regions maintained low apoptosis levels, diminished CD8SP T cells ratios at day 14 versus day 3 may reflect β 5t-mediated selection dynamics(Supplementary Fig. 3). Elevated *Klf6* mRNA levels in regenerated TECs suggests preferential differentiation toward specific mTEC-I subsets, supported by IF results. Ultrastructurally, enhanced tight junctions, nuclear membrane invaginations, autophagosome-containing stromal cells, and aberrant mitochondria were evident at day 3. Sustained high *Sirt3* and *Sirt6* mRNA levels post-regeneration indicate mitochondrial involvement, as

SIRT3 localizes to mitochondria, its upregulation implies RAPA may modulate thymic function through mitochondrial reprogramming (Benigni et al., 2016; Ying et al., 2024).

Post-RAPA thymic regeneration constitutes a complex "rebooting" process involving structural degeneration and functional reconstruction. Endogenous regeneration modestly upregulated β -thymosins, with trends toward increased Tslp and Foxn1 mRNA. This establishes a prerequisite for T-cell reconstitution. But prior evidence indicates endogenous regeneration incompletely restores thymic function(Chaudhry et al., 2016). RAPA-mediated regeneration of the thymus reflects the disadvantage of reduced CD3 + T cells ratio in the periphery.

IL-7 serves as a pivotal cytokine driving thymic regeneration. Combining RAPA with IL-7 enhanced immune reconstitution, compensating for deficits in endogenous recovery. Notably, IL-7 ameliorated sTEC distribution defects in RAPA-treated thymus, increasing capsular thickness and CK8 expression within subcapsular zones vs RR groups. This architectural restoration could support IL-7 potentiates thymocyte differentiation capacity post-RAPA. Mechanistically, co-administration sustained elevated Foxn1 mRNA levels in TECs. IL-7 maintained intercellular adhesion molecule expression while upregulating H2-K1 and $\beta 2m$, creating a pro-survival niche for CD8SP/CD4SP T cells. Although IL-7 did not augment thymosin in the RR2 group, increased Tslp and Foxn1 mRNA levels reflected enhanced regenerative potential. Crucially, DP T cells, which lack IL-7R, exhibited unaltered proportions due to IL-7-mediated apoptosis reduction. Instead, IL-7 primarily expanded mature CD4SP/CD8SP subsets, consistent with prior reports (Napolitano et al., 2003; Wertheimer et al., 2018). IL-7 signaling plays a vital role in regulating thymocyte cell cycle kinetics, can counteract age-related thymic atrophy, and its impairment induces pathological thymic involution (Han et al., 2022; Kuo et al., 2024; Li et al., 2004). Collectively, these findings indicate IL-7 promotes thymic regeneration post-RAPA through, 1) augmented thymocyte proliferation, 2) enhanced TEC-derived regenerative factors.

MET is also an important choice to promote endogenous regeneration and repair of thymus. Combined RAPA-MET administration synergistically enhanced thymic function beyond RAPA monotherapy. This regimen demonstrated superior efficacy in restoring thymic size. Mechanistically, MET augmented tight junction integrity while reducing $T\beta 15$, concurrently sustaining mature CD3⁺TCR β ⁺ T cell proportions. In vitro, RML cultures counteracted RAPA-induced Foxn1 mRNA levels decline in TECs, particularly through Klf6 maintenance. This supports TEC differentiation toward specialized mTEC-I and mTEC-IV subsets (Malin et al., 2023). MET also increased CD34⁺ thymic progenitors and peripheral CD3⁺ T cells, establishing prerequisites for mature T lymphocyte production. Critically, MET ameliorated subcapsular TEC deficiency and enhanced capsular CK8 expression versus RR1/RR2 groups, facilitating early $TCR\alpha\beta^+$ thymocyte maturation (Culberson et al., 2024). Furthermore, RAPA-MET preserved thymic integrity via Sirt3-mediated mechanisms, extending relative telomere length aligning with Yang et al. (2022). Intriguingly, accelerated hair growth post-RAPA potentially links to thymic regeneration (Supplementary Fig. 4).

While this work delineates RAPA-mediated thymic regeneration dynamics, certain limitations warrant acknowledgment. First, the exclusive use of young female mice (6–8 weeks) prioritizes experimental uniformity by minimizing confounders from age-related thymic atrophy and comorbidities. However, this model may not fully recapitulate regeneration processes in aged or immunosenescent contexts. Second, the selection of female groups leverages their attenuated thymic involution trajectory compared to males—a design that controls for androgen-driven thymic suppression while accommodating estrogen's biphasic immunomodulation (Wen et al., 2025; Jia et al., 2023). Nevertheless, sex-specific hormonal influences on TECs remain incompletely characterized herein(Zhou et al., 2025). Future studies should incorporate aging models (e.g. 18–24 month groups) and both sexes to establish RAPA's efficacy across physiological spectra.

While RAPA-mediated thymic involution and regeneration mechanisms require further elucidation, current evidence reveals multifaceted interactions, RAPA directly engages STAT3 or forms FKBP12 complexes to modulate development (Saxton et al., 2017; Sun et al., 2022), while newly identified age-associated TECs (aaTECs) - tightly linked to Foxn1⁺ TEC dynamics – drive degenerative processes. Concurrent shifts in non-epithelial stromal proportions critically impact regenerative capacity(Kousa et al., 2024; Thomas et al., 2020). Morphologically, TEC plasticity underpins thymic homeostasis; cortical TECs depend on medullary paracrine signals for structural integrity-an aging-attenuated process-with TEC contraction constituting an atrophy hallmark (Meireles et al., 2017; Venables et al., 2019). Our observed regeneration featured altered epithelial progenitor ratios and biphenotypic CK5⁺/CK8⁺ TECs (Supplementary Fig. 5), potentially reflecting TEPC-mediated remodeling post-RAPA. Given fluctuating Foxn1 mRNA levels, we propose RAPA may regulate aaTEC proportions. Future studies should delineate RAPA's niche-reprogramming actions through, 1) STAT3/FKBP12 signaling, 2) thymic stromal cell signal crosstalk, and 3) TEPC-driven immune reconstitution pathways. And what kind of way RAPA use to reconstruct immunity is a topic that needs further study in

5. Conclusion

Short-term low dose RAPA induces acute thymic involution via TEC-mediated structural remodeling, while endogenous regeneration post-withdrawal enhances immune competence. IL-7 or MET coadministration during thymic reactivation synergistically elevates TEC functional markers (Foxn1 and Klf6) and Sirt3 mRNA levels, optimizing peripheral immune homeostasis. Transient RAPA exposure initiates a compressed immune reset characterized by disrupted thymocyte and TEC spatial dynamics, potentially underpinning its anti-aging effects. Meanwhile, IL-7/MET combined with RAPA establishes a therapeutic paradigm for T cell reconstitution. These findings highlight combinatorial strategies to mitigate thymic involution while preserving adaptive immune plasticity, offering translational potential for aging-related immunodeficiency therapies.

CRediT authorship contribution statement

Fengjie Zhang: Writing – review & editing, Writing – original draft, Formal analysis. Shiyu Hu: Writing – review & editing, Software, Data curation. Yuyuan Ying: Visualization, Methodology. Meiru Zhou: Formal analysis. Xunuo Wen: Formal analysis. Qingru Sun: Visualization, Methodology. Zhaohuan Lou: Conceptualization. Jianli Gao: Writing – review & editing, Writing – original draft, Supervision, Resources, Funding acquisition.

Fundings

This work was supported by the National Natural Science Foundation of China (grant number, 82474614, 82274621), the research project of Zhejiang Chinese Medical University (grant number, No. 2023JKZDZC06), the project of Science and Technology Department of the State Administration of Traditional Chinese Medicine and Zhejiang Provincial Administration of Traditional Chinese Medicine (GZY-ZJ-KJ-23023) and the Key Laboratory for Diagnosis and Treatment of Upper Limb Edema and Stasis of Breast Cancer.

Declaration of competing interest

The authors declare that they have no known competing financial interests or personal relationships that could have appeared to influence the work reported in this paper.

Acknowledgments

We appreciate the technical support from the Public Platform of Pharmaceutical Research Center and Medical Research Center, Academy of Chinese Medical Science, Zhejiang Chinese Medical University, and the Key Laboratory for Diagnosis and Treatment of Upper Limb Edema and Stasis of Breast Cancer, Hangzhou 310014, China.

Appendix A. Supplementary data

Supplementary data to this article can be found online at https://doi.org/10.1016/j.ejphar.2025.177960.

Data availability

Data will be made available on request.

References

- Abbott, A., 2024. Hacking the immune system could slow ageing here's how. Nature 629 (8011) 276-278. https://doi.org/10.1038/d41586-024-01274-3
- Ashby, K.M., et al., 2023. Author correction, A guide to thymic selection of T cells. Nat. Rev. Immunol. 23, 697. https://doi.org/10.1038/s41577-023-00927-0, 697.
- Barata, J.T., et al., 2019. Flip the coin, IL-7 and IL-7R in health and disease. Nat. Immunol. 20 (12), 1584–1593. https://doi.org/10.1038/s41590-019-0479-x.
- Barros, R.D.S., et al., 2024. Effects of low-dose rapamycin on lymphoid organs of mice prone and resistant to accelerated senescence. Front. Immunol. 15, 1310505. https://doi.org/10.3389/fimmu.2024.1310505.
- Benigni, A., et al., 2016. Mitochondrial dynamics is linked to longevity and protects from end-organ injury, the emerging role of sirtuin 3. Antioxidants Redox Signal. 25 (4), 185–199. https://doi.org/10.1089/ars.2016.6682.
- Bianchi, M.E., et al., 2020. The chemokine receptor CXCR4 in cell proliferation and tissue regeneration. Front. Immunol. 11, 2109. https://doi.org/10.3389/ fimmu.2020.02109.
- Bitto, A., et al., 2016. Transient rapamycin treatment can increase lifespan and healthspan in middle-aged mice. eLife 5, e16351. https://doi.org/10.7554/eLife 16351
- Boehm, T., et al., 2013. Thymus involution and regeneration, two sides of the same coin? Nat. Rev. Immunol. 13, 831–838. https://doi.org/10.1038/nri3534.
- Breed, E.R., et al., 2018. Directing T cell fate, how thymic antigen presenting cells coordinate thymocyte selection. Seminar. Cell Develop. Biol. SI, Antigen Present. 84, 2–10. https://doi.org/10.1016/j.semcdb.2017.07.045.
- Chaudhry, M.S., et al., 2016. Thymus, the next (re)generation. Immunol. Rev. 271, 56-71. https://doi.org/10.1111/imr.12418.
- Chen, C., et al., 2009. mTOR regulation and therapeutic rejuvenation of aging hematopoietic stem cells. Sci. Signal. 2, ra75. https://doi.org/10.1126/ scisignal.2000559.
- Chen, C., et al., 2024. Role of thymosin α1 in restoring immune response in immunological nonresponders living with HIV. BMC Infect. Dis. 24, 97. https://doi. org/10.1186/s12879-024-08985-y.
- Choudhury, D., et al., 2024. Polyploidy and mTOR signaling, a possible molecular link. Cell Commun. Signal. 22, 196. https://doi.org/10.1186/s12964-024-01526-9.
- Cosway, E.J., et al., 2023. The alarmin IL33 orchestrates type 2 immune-mediated control of thymus regeneration. Nat. Commun. 14, 7201. https://doi.org/10.1038/s41467-023-43072-y
- Culberson, E.J., et al., 2024. The cyclin D3 protein enforces monogenic TCRβ expression by mediating TCRβ protein-signaled feedback inhibition of Vβ recombination. J. Immunol. 212, 534–540. https://doi.org/10.4049/jimmunol.2300623.
- Damoiseaux, J.G., et al., 1996. Effect of in vivo rapamycin treatment on de novo T-cell development in relation to induction of autoimmune-like immunopathology in the rat. Transplantation 62 (7), 994–1001. https://doi.org/10.1097/00007890-199610150-00019.
- Duah, M., et al., 2021. Thymus degeneration and regeneration. Front. Immunol. 12, 706244. https://doi.org/10.3389/fimmu.2021.706244.
- Elyahu, Y., Monsonego, A., 2021. Thymus involution sets the clock of the aging T-cell landscape, implications for declined immunity and tissue repair. Ageing Res. Rev. 65, 101231. https://doi.org/10.1016/j.arr.2020.101231.
- Fahy, G.M., et al., 2019. Reversal of epigenetic aging and immunosenescent trends in humans. Aging Cell 18, e13028. https://doi.org/10.1111/acel.13028.
- Graf, M., et al., 2017. Telomere length determines TERRA and R-Loop regulation through the cell cycle. Cell 170, 72–85.e14. https://doi.org/10.1016/j.cell.2017.06.006.
- Han, J., et al., 2022. IL-7 promoted the development of thymic DN3 cells in aged mice via DNA demethylation of Bcl2 and c-Myc genes. Mol. Immunol. 147, 21–29. https://doi.org/10.1016/j.molimm.2022.04.013.
- Heitger, A., et al., 1999. Effective T cell regeneration following high-dose chemotherapy rescued with CD34⁺ cell enriched peripheral blood progenitor cells in children. Bone Marrow Transplant. 23 (4), 347–353. https://doi.org/10.1038/sj.bmt.1701588.
- Hill, R.J., et al., 2024. p53 regulates diverse tissue-specific outcomes to endogenous DNA damage in mice. Nat. Commun. 15, 2518. https://doi.org/10.1038/s41467-024-46844-1.

- Jia, X., et al., 2023. Carya cathayensis leaf extract exerts estrogenic effects on hepatic lipogenesis and adipocytes differentiation in ovariectomized rats fed normal or highfat diets. Clinic. Complement. Med. Pharmacol. https://doi.org/10.1016/j. ccmp_2022_100051
- Juricic, P., et al., 2022. Long-lasting geroprotection from brief rapamycin treatment in early adulthood by persistently increased intestinal autophagy. Nat. Aging 2 (9), 824–836. https://doi.org/10.1038/s43587-022-00278-w.
- Kousa, A.I., et al., 2024. Age-related epithelial defects limit thymic function and regeneration. Nat. Immunol. 25, 1593–1606. https://doi.org/10.1038/s41590-024-01915-9.
- Kraaijeveld, R., et al., 2019. Inhibition of T helper cell differentiation by tacrolimus or sirolimus results in reduced B-Cell activation, effects on T follicular helper cells. Transplant. Proc. 51, 3463–3473. https://doi.org/10.1016/j. transpraced 2010.08.039.
- Kuo, J.F., et al., 2024. Induction of thymus atrophy and disruption of thymocyte development by fipronil through dysregulation of IL-7-Associated genes. Chem. Res. Toxicol. 37 (9), 1488–1500. https://doi.org/10.1021/acs.chemrestox.4c00060.
- Lesniewski, L.A., et al., 2017. Dietary rapamycin supplementation reverses age-related vascular dysfunction and oxidative stress, while modulating nutrient-sensing, cell cycle, and senescence pathways. Aging Cell 16, 17–26. https://doi.org/10.1111/ acel.1254
- Li, L., et al., 2004. IL-12 inhibits thymic involution by enhancing IL-7- and IL-2-induced thymocyte proliferation. J. Immunol. 172 (5), 2909–2916. https://doi.org/10.4049/
- Liang, Z., et al., 2018. MTOR signaling is essential for the development of thymic epithelial cells and the induction of central immune tolerance. Autophagy 14, 505–517. https://doi.org/10.1080/15548627.2017.1376161.
- Liang, Z., et al., 2021. mTORC2 negatively controls the maturation process of medullary thymic epithelial cells by inhibiting the LTβR/RANK-NF-κB axis. J. Cell. Physiol. 236, 4725–4737. https://doi.org/10.1002/jcp.30192.
- Liang, Z., et al., 2022. Age-related thymic involution, mechanisms and functional impact. Aging Cell 21 (8), e13671. https://doi.org/10.1111/acel.13671.
- Liu, Yueping, et al., 2020. Thymosin alpha 1 reduces the mortality of severe coronavirus disease 2019 by restoration of lymphocytopenia and reversion of exhausted T cells. Clin. Infect. Dis. 71, 2150–2157. https://doi.org/10.1093/cid/ciaa630.
- Liu, Z., et al., 2023. Immunosenescence, molecular mechanisms and diseases. Signal Transduct. Targeted Ther. 8, 200. https://doi.org/10.1038/s41392-023-01451-2.
- Lopes, N., et al., 2022. Thymocytes trigger self-antigen-controlling pathways in immature medullary thymic epithelial stages. eLife 11, e69982. https://doi.org/ 10.7554/eLife.69982.
- Malin, J., et al., 2023. Expression of the transcription factor Klf6 by thymic epithelial cells is required for thymus development. Sci. Adv. 9, eadg8126. https://doi.org/ 10.1126/sciadv.adg8126.
- Meireles, C., et al., 2017. Thymic crosstalk restrains the pool of cortical thymic epithelial cells with progenitor properties. Eur. J. Immunol. 47. https://doi.org/10.1002/eji.201746922.
- Miller, J.F.A.P., 2020. The function of the thymus and its impact on modern medicine. Science 369, eaba2429. https://doi.org/10.1126/science.aba2429.
- Nagatake, T., et al., 2021. Selective expression of claudin-5 in thymic endothelial cells regulates the blood-thymus barrier and T-cell export. Int. Immunol. 33, 171–182. https://doi.org/10.1093/intimm/dxaa069.
- Napolitano, L.A., et al., 2003. Effects of IL-7 on early human thymocyte progenitor cells in vitro and in SCID-hu Thy/Liv mice. J. Immunol. 171 (2), 645–654. https://doi. org/10.4049/jimmunol.171.2.645.
- Nitta, T., et al., 2020. Non-epithelial thymic stromal cells, unsung heroes in thymus organogenesis and T cell development. Front. Immunol. 11, 620894. https://doi.org/10.3389/fimmu.2020.620894.
- Nitta, T., Ota, A., Iguchi, T., Muro, R., Takayanagi, H., 2021. The fibroblast, an emerging key player in thymic T cell selection. Immunol. Rev. 302, 68–85. https://doi.org/10.1111/imr.12985.
- Saxton, R.A., et al., 2017. mTOR signaling in growth, metabolism, and disease. Cell 168, 960–976. https://doi.org/10.1016/j.cell.2017.02.004.
- Sharma, H., et al., 2021. Recent advancements in regenerative approaches for thymus rejuvenation. Adv. Sci. (Weinh.) 8, 2100543. https://doi.org/10.1002/ advs.2021.00543
- Shen, J.-M., et al., 2020. Identification and functional study of immortalized mouse thymic epithelial cells. Biochem. Biophys. Res. Commun. 525, 440–446. https://doi. org/10.1016/j.bbrc.2020.02.083.
- Sun, L., et al., 2022. Rapamycin targets STAT3 and impacts c-Myc to suppress tumor growth. Cell Chem. Biol. 29, 373–385.e6. https://doi.org/10.1016/j. chembiol.2021.10.006.
- Takaba, H., et al., 2017. The mechanisms of T cell selection in the thymus. Trends Immunol. 38, 805–816. https://doi.org/10.1016/j.it.2017.07.010.
- Thomas, R., et al., 2020. Contributions of age-related thymic involution to immunosenescence and inflammaging. Immun. Ageing 17, 2. https://doi.org/ 10.1186/s12979-020-0173-8.
- Tong, Q., et al., 2024. Thymocyte migration and emigration. Immunol. Lett. 267, 106861. https://doi.org/10.1016/j.imlet.2024.106861.
- Tong, Q.-Y., et al., 2020. Human thymic involution and aging in humanized mice. Front. Immunol. 11, 1399. https://doi.org/10.3389/fimmu.2020.01399.
- Venables, T., et al., 2019. Dynamic changes in epithelial cell morphology control thymic organ size during atrophy and regeneration. Nat. Commun. 10. https://doi.org/ 10.1038/s41467-019-11879-2.
- Wang, C., et al., 2022. The role of IL-7 and IL-7R in cancer pathophysiology and immunotherapy. Int. J. Mol. Sci. 23, 10412. https://doi.org/10.3390/ijms231810412.

- Wang, J., et al., 2020. CXCR4 antagonist AMD3100 (Plerixafor), from an impurity to a therapeutic agent. Pharmacol. Res. 159, 105010. https://doi.org/10.1016/j. phrs. 2020.105010
- Wang, T., et al., 2020. Research progress on sirtuins family members and cell senescence. Eur. J. Med. Chem. 193. https://doi.org/10.1016/j.ejmech.2020.112207.
- Wang, Y., et al., 2011. Modulation of dietary fat on the toxicological effects in thymus and spleen in BALB/c mice exposed to perfluorooctane sulfonate. Toxicol. Lett. 204, 174–182. https://doi.org/10.1016/j.toxlet.2011.04.029.
- Weichhart, T., 2018. mTOR as regulator of lifespan, aging, and cellular senescence, A mini-review. Gerontology 64, 127–134. https://doi.org/10.1159/000484629.
- Wen, X., et al., 2025. Cytoskeleton proteins, the structural basis of T-lymphocyte and TEC restructure during rapid thymus regeneration. Histol. Histopathol. 18897. https://doi.org/10.14670/HH-18-897. Advance online publication.
- Wertheimer, T., et al., 2018. Production of BMP4 by endothelial cells is crucial for endogenous thymic regeneration. Sci. Immunol. 3, eaal2736. https://doi.org/ 10.1126/sciimmunol.aal2736.
- Wilkinson, J.E., et al., 2012. Rapamycin slows aging in mice. Aging Cell 11, 675–682. https://doi.org/10.1111/j.1474-9726.2012.00832.x.

- Xiao, M.L., et al., 2019. Effects of low-dose rapamycin treatment on lung tissue-resident memory CD8⁺ T cells of mice infected with influenza virus. Immunolog. J. 35 (2), 119–125, 2019. https://doi.10.13431/j.cnki.immunol.j.20190019.
- Xie, F., et al., 2021. Metformin accelerates zebrafish heart regeneration by inducing autophagy. NPJ Regen. Med. 6, 62. https://doi.org/10.1038/s41536-021-00172-w.
- Xu, X., et al., 2024. Ligustilide prevents thymic immune senescence by regulating Thymosin β15-dependent spatial distribution of thymic epithelial cells. Phytomedicine 123, 155216. https://doi.org/10.1016/j.phymed.2023.155216.
- Yang, S.P., et al., 2022. Metformin ameliorates thymus degeneration of mice by regulating mitochondrial function. Int. Immunopharmacol. 108, 108744. https:// doi.org/10.1016/j.intimp.2022.108744.
- Ying, Y., et al., 2024. Thymosin β4 regulates the differentiation of thymocytes by controlling the cytoskeletal rearrangement and mitochondrial transfer of Thymus epithelial cells. Int. J. Mol. Sci. 25, 1088. https://doi.org/10.3390/ijms25021088
- Zhou, M., et al., 2025. Thymus degeneration in women and the influence of female sexual hormones on thymic epithelial cells. Int. J. Mol. Sci. 26 (7), 3014. https://doi. org/10.3390/ijms26073014.
- Zhuo, C., et al., 2022. Mechanistic/mammalian target of rapamycin and side effects of antipsychotics, insights into mechanisms and implications for therapy. Transl. Psychiatry 12, 13. https://doi.org/10.1038/s41398-021-01778-w.